Plant Communications
Research article

CellPress
Partner Journal

Chromosome-level genome assembly of triploid *Cyperus rotundus* uncovers allelic expression patterns and herbicide resistance mechanisms

Lamei Wu[1,2,4], Zi Luo[1,2,4,*], Yanxuan Lu[3], Jiayang Li[3], Min Liu[3], Hailin Cai[1], Shiqin Zhao[3], Jiahao Huang[1], Lei Yi[1], Sifen He[3], Lianyang Bai[1,2,*] and Lang Pan[2,3,*]

[1]Hunan Weed Science Key Laboratory, Hunan Academy of Agricultural Sciences, Changsha 410125, China

[2]Yuelushan Laboratory, Changsha 410128, China

[3]College of Plant Protection, Hunan Agricultural University, Changsha 410128, China

[4]These authors contributed equally to this article.

***Correspondence: Zi Luo (luozi@hunaas.cn), Lianyang Bai (lybai@hunass.cn), Lang Pan (langpan@hunau.edu.cn)**

https://doi.org/10.1016/j.xplc.2025.101624

ABSTRACT

***Cyperus rotundus*, a globally distributed and highly competitive weed, has evolved herbicide resistance, posing a significant challenge to sustainable agriculture; however, the lack of genomic resources has limited comprehensive investigations into its resistance mechanisms. Here, we report a chromosome-level genome assembly of triploid *C. rotundus* (875.13 Mb across 165 chromosomes), which exhibits high synteny among haplotypes. Comparative analysis of six populations revealed that only a population from Changde, Hunan, China (designated R-HN) displayed dual resistance to glyphosate and glufosinate. In this population, high expression of the target-site resistance gene *glutamine synthetase 2* (*GS2*) contributes to glufosinate resistance, whereas glyphosate resistance is predominantly mediated by non-target-site resistance (NTSR) mechanisms. By integrating transcriptomic profiling with yeast-based functional validation, we identified two NTSR genes, *CrABCG15* and *CrCASPL2C2*, that confer glyphosate resistance. Collectively, this study provides a high-quality genomic resource for *C. rotundus* and advances our understanding of its genomic evolution and herbicide resistance mechanisms.**

Key words: *Cyperus rotundus*, genome assembly, herbicide resistance, glyphosate non-target-site resistance, (NTSR), *glutamine synthetase 2* (*GS2*) overexpression.

Wu L., Luo Z., Lu Y., Li J., Liu M., Cai H., Zhao S., Huang J., Yi L., He S., Bai L., and Pan L. (2026). Chromosome-level genome assembly of triploid *Cyperus rotundus* uncovers allelic expression patterns and herbicide resistance mechanisms. Plant Comm. **7**, 101624.

INTRODUCTION

It is noteworthy that weeds competing with crops can cause average annual yield losses exceeding 20% across a range of agronomic and horticultural crops (Oerke, 2006; Soltani et al., 2016; Peerzada, 2017). *Cyperus rotundus*, a perennial herbaceous species in the Cyperaceae family, is widely distributed in temperate, tropical, and sub-tropical regions and occupies diverse habitats, including both agricultural and non-agricultural fields (Xue et al., 2023). Agriculturally, *C. rotundus* is considered one of the most invasive and economically damaging weeds (Bendixen and Nandihalli, 1987). Through intense resource competition, it causes substantial yield reductions in major crops, including seeded rice (Chauhan and Opeña, 2012), maize (Atwell et al., 1985), soybean, cotton (Webster and Macdonald, 2001), and sugarcane (Chand et al., 2013), thereby posing a significant threat to agricultural ecosystems. Unlike most weeds, *C. rotundus* primarily propagates through underground tubers and basal bulbs, with seeds contributing minimally to reproduction (Neeser et al., 1997). Its rapid vegetative growth, extensive subterranean rhizome network, and C_4 photosynthetic efficiency confer a strong competitive advantage (Lati et al., 2011), making effective management particularly challenging.

Genomes of many domesticated crop varieties and their wild relatives have been sequenced, significantly improving our understanding of the genetic basis of critical agronomic traits (Michael and VanBuren, 2015). In contrast, genomic analyses of agricultural weed species have historically lagged behind, despite their considerable economic impact. Nevertheless, genomic approaches provide a robust framework for identifying the origins of invasive weed species and uncovering adaptive

alleles, thereby providing a foundation for developing targeted weed management strategies. Recent advances in sequencing technologies, coupled with increasing agricultural threats, have facilitated the assembly of genomes for 32 weed species (Chen et al., 2024b), although many remain at sub-chromosomal resolution, leaving key genetic mechanisms of weed adaptation poorly understood. Furthermore, the International Weed Genomics Consortium (IWGC) has completed or is currently conducting genome assemblies for 31 weed species, primarily focusing on crop-associated weeds (Montgomery et al., 2024). Most sequenced weeds are diploid, with only a few tetraploid and hexaploid species. *C. rotundus*, a globally problematic triploid weed, has attracted attention from the IWGC (Montgomery et al., 2024). However, the absence of a reference genome has severely limited genomic and genetic research on this highly invasive species.

Polyploidy is a major driver of plant genome evolution and species diversification (Adams and Wendel, 2005), facilitating ecological adaptation by increasing genetic variation and divergence among subgenomes (Freeling et al., 2015). Polyploidy is particularly prevalent in weeds, with species such as *Leptochloa chinensis* (Wang et al., 2022), *Echinochloa crus-galli* (Guo et al., 2017), and *Capsella bursa-pastoris* (Kasianov et al., 2017) exhibiting polyploid genomes. Polyploids often display enhanced tolerance to abiotic stresses (DaiYin et al., 2013), and gene duplication, particularly copy-number variation in herbicide target-site resistance (TSR) genes, has been implicated in promoting adaptive resistance under herbicide selection (Chen et al., 2023; Johnson et al., 2024). However, triploids remain poorly characterized, largely due to meiotic instability. Triploid genome assemblies have been reported in species such as *Lilium* "Triumphator" (LLO) (Cui et al., 2022), *Cavendish banana* (Huang et al., 2023), and *Populus* species (Tong et al., 2022), but triploid weeds remain unexplored. *C. rotundus*, a putative triploid hybrid that primarily propagates through tubers, lacks a chromosome-scale reference genome. Advances in sequencing technologies now provide an unprecedented opportunity to elucidate the subgenome dynamics underlying its invasiveness.

Herbicide resistance represents a key adaptive trait that may evolve in plant populations subjected to agricultural selection pressures. Over-reliance on herbicides, coupled with low diversity and insufficient redundancy in weed management strategies, has contributed to the global spread of herbicide resistance (Consortium, 2013). Resistance can arise through multiple physiological mechanisms, broadly categorized into TSR and non-target-site resistance (NTSR) (Powles and Yu, 2010). TSR involves alterations that reduce the binding affinity between a herbicide and its target protein (Lonhienne et al., 2022). In contrast, NTSR comprises modifications in herbicide absorption, translocation, sequestration, and/or metabolism, which may produce unpredictable pleiotropic cross-resistance, rendering structurally and functionally diverse herbicides ineffective due to one or more genetic variants (Dimaano et al., 2020). Genomic resources can be utilized to predict the protein structures of novel herbicide target-site and metabolism genes, thereby enhancing our understanding of NTSR mechanisms. NTSR involves genes with diverse biochemical functions, many of which belong to large and complex gene families (Delye et al., 2011; Comont et al., 2022). Untargeted approaches, including genome-wide association studies, selective sweep scans, linkage mapping, RNA sequencing, and metabolomic profiling, have proven invaluable for complementing targeted biochemical and chemotypic studies aimed at elucidating NTSR mechanisms (Han et al., 2021; Gupta et al., 2023; Qiao et al., 2023), all of which rely on high-quality genomic data.

Glyphosate and glufosinate have been widely used to control *C. rotundus* (Charles, 1995; Agahiu, 2020); however, repeated application has led to the emergence of glyphosate- and glufosinate-resistant populations. Glyphosate inhibits 5-enolpyruvylshikimate-3-phosphate synthase (EPSPS), disrupting aromatic amino acid biosynthesis and ultimately causing plant death (Hollander and Amrhein, 1980; Gaines et al., 2019). TSR mechanisms include single mutations (Pro-106-Ser/His/Ala/Thr) (Chen et al., 2015; Loddo et al., 2020; McElroy and Hall, 2020; Yanniccari et al., 2022), double mutations (Thr-102-Ile + Pro-106-Ser) (Yu et al., 2015), and triple mutations (Thr-102-Ile + Ala-103-Val + Pro-106-Ser) (Perotti et al., 2019), as well as EPSPS gene amplification. NTSR mechanisms involve detoxification enzymes, including cytochrome P450s (EiCYP71AK44 in *Eleusine indica* [He et al., 2024]), aldo-keto reductases (EcAKR4-*1* in *Echinochloa colona* [Pan et al., 2019], LrAKR4C10 and LrAKR1 in *Lolium rigidum* [Zhou et al., 2023]), and ABC transporters (EcABCC8 in *Echinochloa colona* [Pan et al., 2021]), which mediate glyphosate metabolism and transport. Glufosinate, in contrast, inhibits glutamine synthetase (GS), causing ammonia accumulation, chloroplast disruption, and impaired carbon assimilation (Edwards and Coruzzi, 1989; Weber and Flügge, 2002). TSR to glufosinate has been linked to *glutamine synthetase 2* (*GS2*) amplification and overexpression in *Amaranthus palmeri* (Carvalho-Moore et al., 2022, 2025; Noguera et al., 2022, 2024), as well as point mutations, such as Ser-59-Gly in *Eleusine indica* (Zhang et al., 2022). To date, no mechanisms conferring glyphosate or glufosinate resistance have been reported in *C. rotundus*.

Here, we generated a chromosome-level assembly of the triploid *C. rotundus* genome. Using comparative genomics, we investigated the origins and evolutionary history of *C. rotundus*. Six populations were collected, including the genome-sequenced S-YN population (from Xishuangbanna, Yunnan, China); notably, only the R-HN population (from Changde, Hunan, China) exhibited resistance to both glyphosate and glufosinate compared with S-YN. We characterized the dynamic expression patterns of homoeologous triads in S-YN and R-HN populations and examined NTSR-associated gene families, including *ABC transporters*, *AKRs*, and *CYP450s*. Furthermore, amplification and high expression of *GS* genes were observed, contributing to glufosinate resistance, whereas glyphosate resistance was mediated primarily through NTSR mechanisms. By integrating transcriptomic data from S-YN and R-HN, evaluating expression patterns at multiple time points following glyphosate treatment, and performing molecular docking and functional validation in yeast, we identified candidate genes that confer glyphosate resistance. This study provides a high-quality genomic resource for understanding the adaptation of triploid weeds and offers insights into the genetic mechanisms underlying herbicide resistance in *C. rotundus*, thereby supporting the development of targeted weed management strategies.

RESULTS

Genome assembly and annotation of *C. rotundus*

Prior to de novo assembly, k-mer frequency analysis indicated that *C. rotundus* is polyploid (supplemental Figure 1). The estimated haploid genome size was 306.39 Mb, later refined to 297.64 Mb, with a heterozygosity rate of 2.25% and 41.14% repetitive sequences. To generate a high-quality *C. rotundus* genome assembly, we sequenced a population from Xishuangbanna, Yunnan, China (S-YN), using PacBio HiFi and Hi-C technologies, generating 102.89 Gb of HiFi reads (∼117.6× coverage of the total genome size) and 99.54 Gb of Hi-C reads (∼113.7× coverage of the total genome size).

The *C. rotundus* genome was assembled using HiFi sequencing for de novo assembly with Hifiasm, producing an initial contig-level assembly of 1282.59 Mb with a contig N50 of 3.02 Mb. Subsequent Hi-C scaffolding anchored the contigs into pseudochromosomes (supplemental Figure 2A), achieving a Hi-C mapping rate of 95.69% and correcting structural errors. The final chromosome-level assembly spanned 875.13 Mb, with a contig N50 of 4.07 Mb, comprising 165 chromosomes (55 per haplotype, designated hapI, hapII, and hapIII) (supplemental Figure 2B). To evaluate genome completeness and accuracy, multiple quality assessment approaches were employed. HiFi read mapping demonstrated a 99.94% alignment rate and 99.95% genome coverage (supplemental Table 1). Long terminal repeat (LTR) Assembly Index (LAI) scores were 13.43, 15.16, and 14.82 across hapI, hapII, and hapIII, respectively (supplemental Table 1). BUSCO analysis revealed that complete sequences accounted for 93.2%, 93.2%, and 92.8% of the conserved core eukaryotic gene set in hapI, hapII, and hapIII, respectively (supplemental Figure 2C). Collectively, these metrics indicate that the *C. rotundus* reference genome is of high quality, accuracy, and reliability.

Genome annotation identified protein-coding genes, repetitive sequences, and non-coding RNAs. Using homology-based, ab initio, and transcriptome-based prediction approaches, we annotated a total of 72,354 protein-coding genes, with an average gene length of 3,623 bp, an average coding sequence length of 1,258 bp, and an average of five exons per gene (supplemental Table 2). To validate gene annotations, InterPro was employed for protein domain analysis, revealing functional domains in approximately 80% (57,946) of the genes. Comparative analysis with closely related species confirmed the consistency of coding genes, coding sequences, exons, and introns (supplemental Figure 3). Repetitive sequence annotation identified approximately 452 Mb (51.57%) of the genome as transposable elements (TEs), with LTR elements being the most abundant, accounting for 33.79% of the genome (supplemental Table 2). Analysis of genomic feature distribution revealed a reduction in LTR element content in gene-rich regions. Non-coding RNA annotation identified 209 miRNAs, 1,480 tRNAs, 4,785 rRNAs, and 292 snRNAs (supplemental Table 2).

The assembled sizes of the three haplotypes, hapI, hapII, and hapIII, were 289.15, 278.23, and 270.09 Mb, respectively (supplemental Table 3). All assemblies exhibited high continuity, with only a few gaps ranging from 37 to 84 (supplemental Table 3). Repeat content was comparable across haplotypes, accounting for 51.45%–53.24% of each. Gene prediction analyses identified 23,362, 23,007, and 22,736 protein-coding genes in hapI, hapII, and hapIII, respectively. Strong collinearity was observed among the three haplotypes, with no evidence of major chromosomal rearrangements (Figure 1A). Collectively, these results indicate that the haplotypes maintain high structural conservation and a stable genomic architecture.

Genome evolution of *C. rotundus*

To further investigate the evolutionary relationships of *C. rotundus* with other species, we performed gene family clustering using representatives from the genus *Cyperus*, other Cyperaceae species, and the outgroup *Arabidopsis thaliana*. Gene families were clustered based on sequence homology (supplemental Figure 4A; supplemental Table 4), revealing that 8,757 core gene families are shared among the four species (*C. rotundus*, *Arabidopsis thaliana*, *Cyperus esculentus*, and *Rhynchospora breviuscula*), whereas 706 gene families are specific to *C. rotundus* (supplemental Figure 4B). Phylogenetic reconstruction and divergence time estimation were conducted using single-copy orthologs shared among these species. The analysis indicates that *C. rotundus*, *Cyperus esculentus*, *Carex littledalei*, and *Rhynchospora breviuscula* form a distinct phylogenetic branch within the Cyperaceae Juss. (Figure 1B). Notably, *C. rotundus* and *Cyperus esculentus* share the closest phylogenetic relationship, diverging from a common ancestor approximately 19 million years ago (Figure 1B).

Gene family expansion and contraction have played pivotal roles in adaptive diversification, reflecting the remarkable ecological plasticity of *C. rotundus.* Phylogenetic analysis identified 448 expanded and 370 contracted gene families in *C. rotundus (*Figure 1B). Functional enrichment analysis revealed that contracted gene families are primarily involved in essential cellular processes, including endocytosis, ubiquitin-mediated proteolysis, and starch and sucrose metabolism (Figure 1C; supplemental Figure 5). Protein annotation further indicated that these genes predominantly encode acetyltransferases, along with auxiliary proteins such as SAUR36, multiple hypothetical proteins, and components of the exocyst complex (supplemental Table 5). In contrast, expanded gene families were significantly enriched in pathways related to secondary metabolite biosynthesis, including diterpenoid, flavone/flavonol, pantothenate, CoA, and carotenoid biosynthesis, as well as circadian rhythm regulation (Figure 1D). These gene families are predominantly composed of GDSL esterases/lipases, receptor-like kinases, polygalacturonase inhibitors, F-box/LRR-repeat proteins, and early light-induced proteins, with a smaller fraction represented by gibberellin-related proteins, MYB DNA-binding proteins, and disease resistance proteins (supplemental Table 5). Gene Ontology (GO) enrichment analysis further revealed an overrepresentation of functions associated with transmembrane signaling, ion transport, and nucleic acid metabolism, including G-protein-coupled receptor activity, ligand-gated ion channel activity, and ribonuclease activity (supplemental Figure 6). These expansions suggest that C. rotundus has evolved enhanced capabilities for environmental sensing, signal transduction, and chemical defense, likely contributing to its invasiveness and ecological competitiveness under diverse and stressful conditions.

To investigate the adaptive evolutionary mechanisms of *C. rotundus*, we performed a genome-wide scan for positive selection using

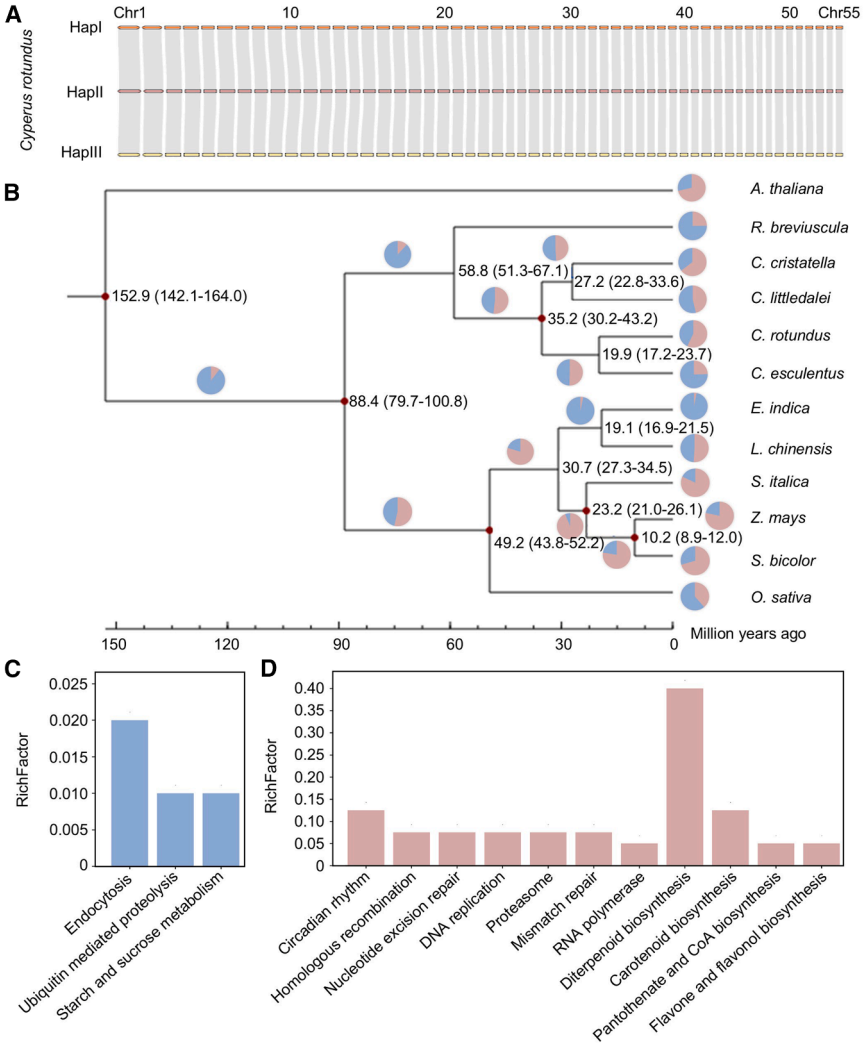

Figure 1. Comparative evolution of *Cyperus rotundus* (*C. rotundus*).

(A) Sequence collinearity among hapI, hapII, and hapIII.

(B) Phylogenetic relationships and divergence times between *C. rotundus* and other species. Expanded gene families are shown in pink pie charts, whereas contracted gene families are shown in blue pie charts.

(C and D) Enriched KEGG pathways in contracted **(C)** and expanded **(D)** gene families of *C. rotundus*.

Ka/Ks analysis, identifying 80 genes potentially subjected to selective pressure (supplemental Table 6). KEGG enrichment analysis indicated that these genes are significantly involved in pathways related to cell growth and death, transport and catabolism, and various metabolic processes, particularly carbohydrate and vitamin metabolism (supplemental Figure 7). GO enrichment analysis further supported these findings, showing that positively selected genes are predominantly associated with biological processes such as response to stimulus, cellular component organization, developmental processes, and metabolic regulation (supplemental Figure 8). Additionally, a substantial proportion of these genes are localized to key cellular components, including membranes, organelles, and macromolecular complexes, and are enriched for molecular functions such as catalytic activity and binding (supplemental Figure 8). Collectively, these results indicate that positive selection in *C. rotundus* has targeted genes essential for cellular homeostasis, stress response, and metabolic plasticity.

The R-HN population confers resistance to glyphosate and glufosinate in *C. rotundus*

In addition to the genome-sequenced population (S-YN), five other *C. rotundus* populations, designated CS, HN, HB, HeN, and ZJ, were collected and evaluated for glyphosate and glufosinate sensitivity. Dose-response assays revealed pronounced regional variation in glyphosate resistance. The Yunnan population, sourced from fields with no prior glyphosate or glufosinate application, had a GR_{50} of 3603.86 g a.i./ha and served as the reference (resistance index [RI] = 1.00) (Table 1). The CS, HB, HeN, and ZJ populations displayed similar sensitivity, with GR_{50} values ranging from 3646.97 to 4146.66 g a.i./ha and relative resistance indices between 1.01 and 1.15 (Table 1). In contrast, the HN population, originating from a vegetable field with a history of repeated glyphosate application, exhibited the highest resistance, with a GR_{50} of 8897.36 g a.i./ha, corresponding to a 2.47-fold increase relative to the reference (Table 1).

Similarly, dose-response assays were conducted to assess glufosinate resistance levels among various *C. rotundus* populations. The Yunnan population exhibited a GR_{50} of 909.70 g a.i./ha, serving as the reference (RI = 1.00) (Table 1). The CS, HB, HeN, and ZJ populations showed GR_{50} values ranging from 960.05 to 1037.74 g a.i./ha, with relative resistance indices fluctuating between 1.06 and 1.14 (Table 1). The HN population again displayed the highest resistance, with a GR_{50} of 2161.11 g a.i./ha, corresponding to a 2.38-fold increase relative to the reference (Table 1). Collectively, these results demonstrate that the HN population (designated R-HN) exhibits dual resistance to both glyphosate and glufosinate compared with the Yunnan population (S-YN).

High expression of *GS2* in the R-HN population of *C. rotundus*

RNA-seq analysis was performed on leaf samples from untreated S-YN and R-HN populations at the four- to five-leaf stage. A total of 16,094 differentially expressed genes (DEGs) were identified, including 6,080 upregulated and 10,014 downregulated genes (supplemental Figure 9A; supplemental Table 7).

Protein sequence alignment identified three *GS2* homologs in the *C. rotundus* genome corresponding to the rice *GS2* gene (*LOC_Os10g31820*). *GS2* (*LOC_Os10g31820*) aligned to three candidate gene copies in *C. rotundus*, forming a homoeologous triad

Herbicides	Population	Dose-response regression equation	Correlation coefficient (R)	Growth reduction 50% (GR50) (g a.i./ha m^2)	Relative resistance level
Glyphosate	YN	y = −0.2906 + 1.4875x	0.96	3603.86 (2418.00–5371.34)	1
	HN	y = −2.3372 + 1.8579x	0.99	8897.36 (8422.40–9399.11)	2.47
	CS	y = 0.1959 + 1.3435x	0.87	3764.72 (2482.87–5708.36)	1.04
	HB	y = 0.8423 + 1.1493x	0.98	4146.66 (3576.31–4807.96)	1.15
	HeN	y = 1.4240 + 0.9915x	0.91	4043.02 (2926.48–5585.56)	1.12
	ZJ	y = 1.1984 + 1.0673x	0.96	3646.97 (2930.96–4537.90)	1.01
Glufosinate	YN	y = 1.8487 + 1.0650x	0.96	909.70 (721.53–1146.93)	1
	HN	y = 0.7020 + 1.2889x	0.92	2161.11 (1614.90–2892.05)	2.38
	CS	y = 0.9811 + 1.3420x	0.98	987.85 (867.73–1124.59)	1.09
	HB	y = 0.9045 + 1.3656x	0.97	998.08 (823.56–1209.58)	1.1
	HeN	y = 1.2132 + 1.2555x	0.96	1037.74 (848.87–1268.64)	1.14
	ZJ	y = 1.0984 + 1.3083x	0.92	960.05 (704.01–1309.20)	1.06

Table 1. Relative resistance levels of *C. rotundus* populations to glyphosate and glufosinate.

located on chromosome 55 in hapI, hapII, and hapIII (Figure 2A; supplemental Table 8). Transcriptome visualization of the S-YN and R-HN populations revealed no amino acid substitutions at codons Ser59 or Asp171 (supplemental Figure 10A), positions previously associated with GS sequence variation (Avila-Garcia et al., 2012; Zhang et al., 2022). Genomic DNA-based qPCR confirmed no significant differences in *GS2* copy number between S-YN and R-HN, indicating that gene amplification does not contribute to differential expression (supplemental Figure 10B). To investigate the expression patterns of *GS* alleles, we compared their expression levels between the S-YN and R-HN populations. Notably, *Cro69233* (*GS2* homoeolog) was significantly upregulated in the R-HN population, with the remaining homoeologs showing no significant differences (Figure 2B). Quantitative real-time PCR (RT-qPCR) performed on both RNA-seq samples and independent biological replicates corroborated the upregulation of *Cro69233*, supporting the RNA-seq findings (Figure 2C; supplemental Table 9). These findings suggest that overexpression of *GS* genes may confer glufosinate resistance, consistent with previous reports (Chen et al., 2024a).

BLASTp and BLASTn alignment analyses identified three *EPSPS* genes in the *C. rotundus* genome, exhibiting high homology with the GenBank reference sequence (DQ153168.2) (supplemental Table 12). These EPSPS genes are organized into three haplotypes (hapI, hapII, hapIII) located on chromosome 53 (Figure 2D; supplemental Table 10). Visualization of transcriptome data from the S-YN and R-HN populations revealed no amino acid substitutions at the Thr102, Ala103, and Pro106 codons (supplemental Figure 11), which are commonly reported positions for changes in the EPSPS enzyme sequence. Differential expression analysis revealed that one *EPSPS* allele, *Cro68444*, was significantly downregulated in R-HN, whereas the other two homologs maintained stable expression levels (Figure 2E). These findings support the conclusion that glyphosate resistance in the R-HN population is not mediated by TSR but rather through NTSR mechanisms, motivating the subsequent identification of candidate NTSR genes involved in glyphosate resistance.

Allelic expression patterns in the triploid *C. rotundus* genome

To investigate allele-specific expression in *C. rotundus*, we identified 14,244 allelic triads in the genome, each displaying a 1:1:1 correspondence across the three haploid genome assemblies (supplemental Table 11). In the S-YN population, 10,761 triads (75.55% of all triads) were expressed, encompassing 32,283 genes (Figure 3A; supplemental Table 12), with at least one allele exhibiting an expression level above 0.5. The relative expression of hapI, hapII, and hapIII alleles was normalized and analyzed globally (Figure 3B). In S-YN, 3,820 triads (~35.5%) displayed unbalanced expression, with dominant triads per haplotype ranging from 111 to 163 and suppressed triads ranging from 1, 124 to 1,163 (Figure 3A and 3B; supplemental Table 12). In the R-HN population, 30,747 expressed genes (10,249 allelic triads) were examined, of which 7,957 triads (approximately 77.6%) displayed an unbalanced expression pattern (Figure 3C; supplemental Table 13). The number of dominant triads per haplotype ranged from 322 to 448, while the number of suppressed triads ranged from 1,862 to 2,542 (Figure 3D; supplemental Table 13). Of the 10,761 expressed triads in S-YN, 9,561 (88.8%) were also expressed in R-HN (supplemental Figure 12A). In addition, 1,200 triads were exclusively expressed in S-YN but silenced in R-HN, whereas 688 triads were uniquely

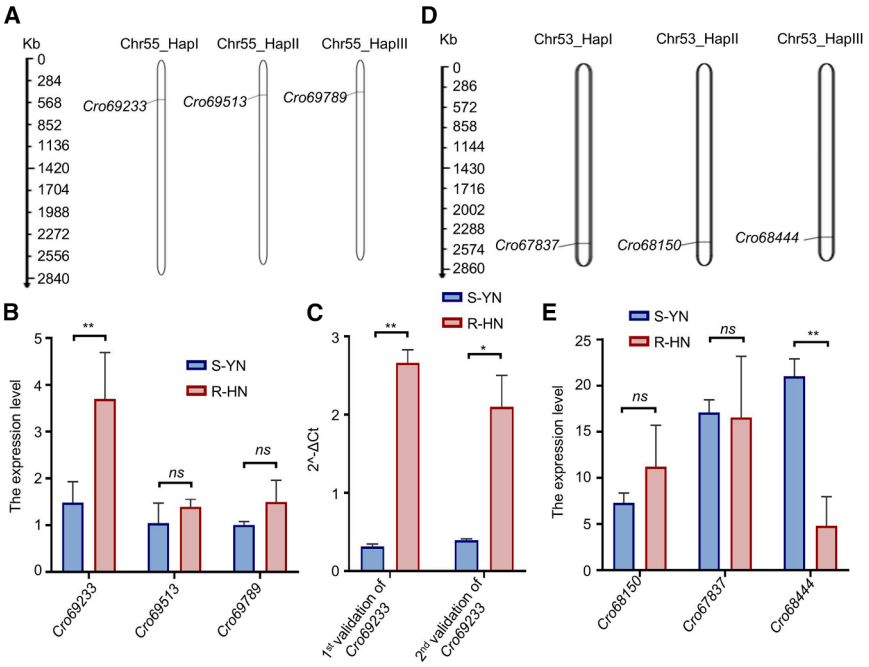

Figure 2. Genomic distribution and expression profiles of *EPSPS* and *GS* homoeologs in *Cyperus rotundus*.

(A) Chromosomal locations of *GS2* genes.

(B) Transcript abundance (FPKM) of *GS2* homoeologs in the R-HN and S-YN populations. Significant differences are defined as $|\log_2(\text{fold change})| \geq 1$ and FDR < 0.05 using DESeq2 (ns, not significant).

(C) RT-qPCR validation of overexpressed *GS2* genes. Red indicates the R-HN population, blue indicates the S-YN population. Significance was determined by Student's *t-test* (*p < 0.05; ** $p < 0.01$; ns, not significant).

(D) Chromosomal locations of *EPSPS* genes.

(E) Transcript abundance (FPKM) of *EPSPS* homoeologs in the R-HN and S-YN populations. **Significant differences are defined as $|\log_2(\text{fold change})| \geq 1$ and FDR < 0.05 by DESeq2 (ns, not significant).

upregulated in R-HN (supplemental Figure 12A). Genes specifically expressed in allelic triads of the S-YN population are enriched in pathways related to plant growth and development, including the regulation of flower development, root development, amino acid biosynthesis, chloroplast stroma, and cytokinin metabolism (supplemental Figure 12B). In contrast, triads uniquely expressed in R-HN are enriched in pathways related to leaf senescence, glutamine metabolism, and response to hydrogen peroxide, suggesting a role in stress adaptation and herbicide resistance (supplemental Figure 12C).

Allelic genes within balanced triads contributed equally to overall expression (Figure 3B and 3D). Our analysis revealed that the proportion of balanced triads decreased dramatically from 64.5% in the S-YN population to 22.4% in the R-HN population (Figure 3E). In comparison with the S-YN population, the overall frequency of dominant triads (hapXgeneD) was significantly higher in the R-HN population, with hapIgeneD increasing from 1.27% to 4.37%, hapIIgeneD from 1.03% to 3.40%, and hapIIIgeneD from 1.05% to 3.14% (Figure 3E). In these dominant triads, one allele exhibited markedly higher expression than the other two alleles observed in balanced triads (Figure 3F). Additionally, the frequency of suppressed triads increased substantially in R-HN, with hapIgeneS increasing from 10.81% to 18.17%, hapIIgeneS from 10.89% to 23.76%, and hapIIIgeneS from 10.45% to 24.80% (Figure 3E). In these suppressed triads, one allele displayed significantly lower transcript abundance relative to the other alleles (Figure 3F). Collectively, these findings demonstrate substantial shifts in allelic expression patterns between the S-YN and R-HN populations.

Allelic expression bias of DEGs between S-YN and R-HN populations

Functional enrichment analysis revealed that genes upregulated in R-HN were predominantly enriched in GO terms associated with key biological processes, including amine biosynthesis, photomorphogenesis, response to endoplasmic reticulum stress, peroxisome and microbody components, photosynthesis, light stimulus response, phosphatase and phosphoric ester hydrolase activities, small-molecule metabolism, response to abiotic stimuli, general metabolic processes, and catalytic activity (supplemental Figure 9B). Conversely, downregulated genes were primarily enriched in GO terms related to RNA binding, intracellular and vesicle-mediated transport, nitrogen compound and peptide metabolism, ADP binding, macromolecule localization, catalytic complexes, and mRNA metabolic processes (supplemental Figure 9C).

Triploidization in *C. rotundus* has led to the presence of gene triads, necessitating further analysis of allelic expression dynamics among DEGs in the R-HN population. Of all DEGs, 66,835 triads were expressed in the S-YN population, whereas 66,407 triads were expressed in the R-HN population (fragments per kilobase of transcript per million mapped reads [FPKM] > 0.5). Notably, in S-YN, approximately 67% of triads exhibited a balanced expression pattern, whereas in R-HN, this proportion dropped sharply to 11.76%, accompanied by a shift toward dominant and suppressed expression patterns, with HapXgeneS patterns accounting for 75.56% in R-HN (Figure 4A). Comparative analysis of allelic expression dynamics between the two populations revealed that only 919 triads maintained consistent expression patterns, whereas 4,163 balanced triads in the S-YN population shifted to alternative pattern types in the R-HN population (Figure 4B; supplemental Table 14). These shifts were accompanied by significant up- or downregulation of allelic expression.

Using the known glyphosate resistance genes *EcABCC8* and *EcAKR4-1* as examples, *EcABCC8* in *C. rotundus* comprised two allelic triads (six genes total). One triad maintained a balanced expression pattern across both populations, with all alleles showing stable upregulation in R-HN (Figure 4C). In contrast, the other triad shifted from a hapIgeneS pattern in the S-YN population to a balanced pattern in the R-HN population (Figure 4C). Six alleles of *ABCC8* were present, with one allele downregulated and three

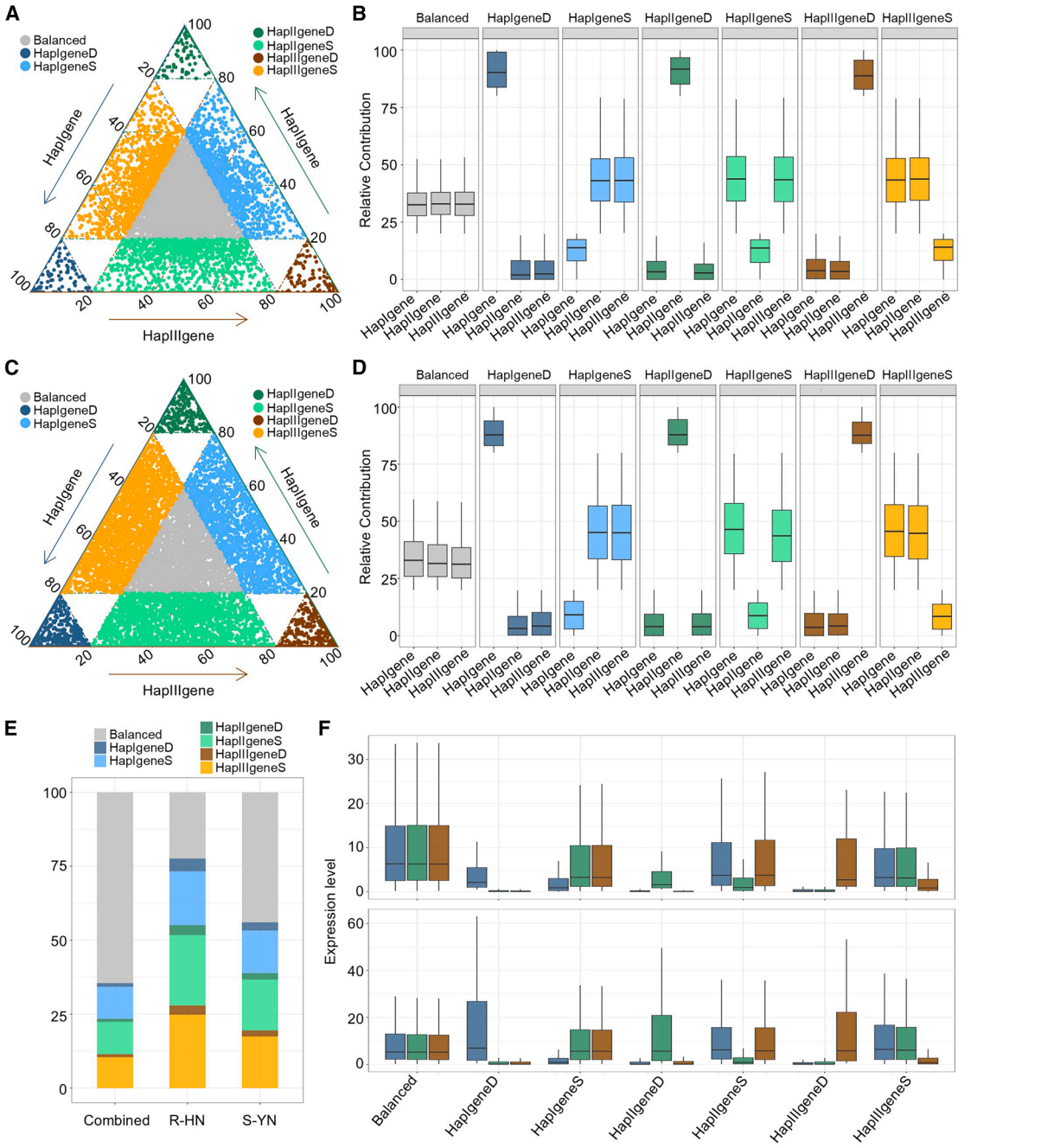

Figure 3. Allelic expression bias in syntenic allelic triads.

(A) Ternary plot showing relative expression levels of 10,761 allelic triads (32,283 genes) in the S-YN population. Each point represents a gene triad, with hapI, hapII, and hapIII coordinates reflecting the relative contribution of each allele. Gray points indicate balanced triads; colored points at vertices indicate allele-dominant triads; colored points along edges or intermediate regions indicate allele-suppressed triads.

(B) Boxplots showing relative allele contributions across seven triad categories in S-YN. Specifically, hapIgeneD, hapIIgeneD, and hapIIIgeneD represent hapI-, hapII-, and hapIII-dominant triads, respectively, whereas hapIgeneS, hapIIgeneS, and hapIIIgeneS represent hapI-, hapII-, and hapIII-suppressed triads.

(C) Ternary plot of 10,249 allelic triads (30,747 genes) in the R-HN population.

(D) Boxplots of relative allele contributions across the seven triad categories in R-HN.

(E) Comparative analysis of allelic expression bias among S-YN, R-HN, and the combined dataset.

(F) Boxplots showing absolute transcript abundance for each haploid genome across the seven allelic triad categories in the S-YN (top) and R-HN (bottom) populations.

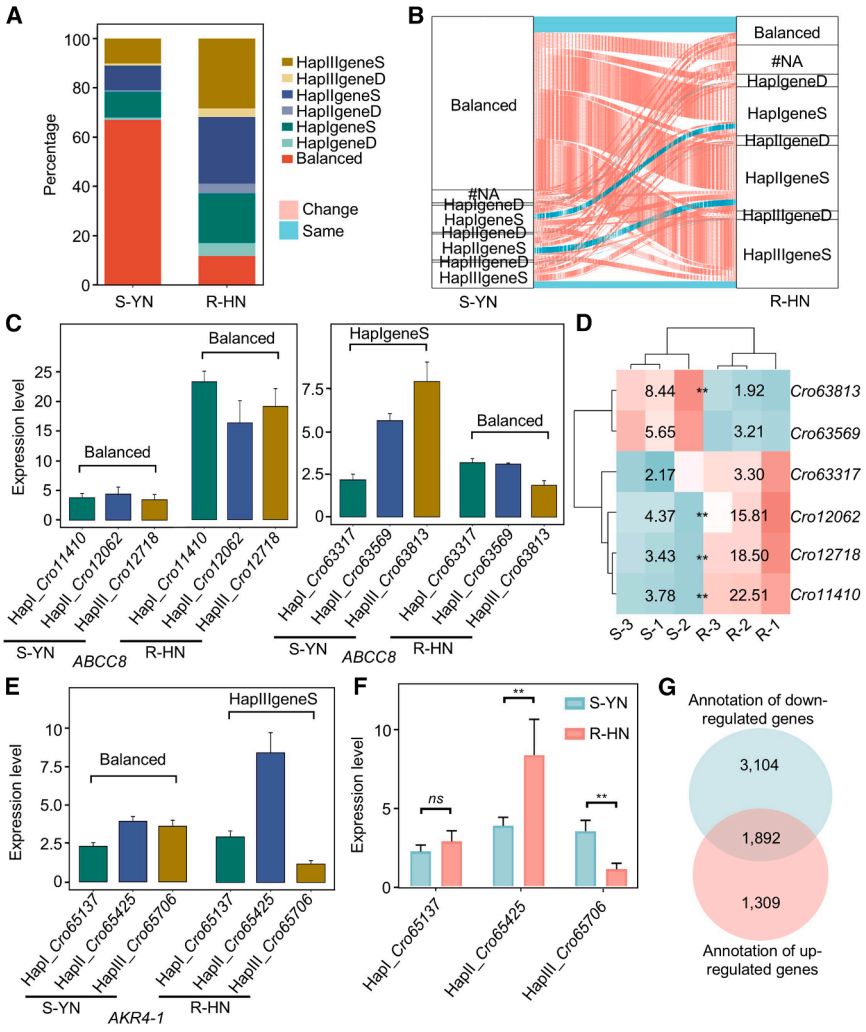

Figure 4. Differential expansion and allelic expression patterns of differentially expressed genes (DEGs) between the S-YN and R-HN populations of *C. rotundus*.

(A) Comparative analysis of allelic expression bias among DEGs in the S-YN and R-HN populations.

(B) Sankey diagram showing dynamic shifts in expression patterns of DEGs between the S-YN and R-HN populations.

(C and D) Allelic expression bias **(C)** and expression levels **(D)** of *ABCC8* in the S-YN and R-HN populations. Numbers in the heatmap indicate average expression levels. ** indicates statistically significant differences in expression levels.

(E and F) Allelic expression bias **(E)** and expression levels **(F)** of *AKR4-1* in the S-YN and R-HN populations. Red and green indicate the R-HN and S-YN populations, respectively. ** indicate significant differences determined by DESeq2 ($|\log_2(\text{fold change})| \geq 1$ and FDR < 0.05). ns, not significant.

(G) Venn diagram showing the overlap of allele annotations between upregulated and downregulated gene sets.

alleles upregulated (Figure 4D). Similarly, *EcAKR4-1* in *C. rotundus* comprised one expressed allelic triad, which displayed a balanced expression pattern in S-YN but shifted to a hapIIIgeneS pattern in R-HN (Figure 4E), with one allele downregulated and one upregulated (Figure 4F). These shifts in triad expression patterns highlight the complex regulation of allelic expression in R-HN, demonstrating that shifts in triad patterns can result in concurrent up- and downregulation of different alleles.

At the genome-wide level, we observed that among the upregulated genes, 4,429 allelic counterparts were simultaneously downregulated in the R-HN population (Figure 4G). This complex divergence in triad expression complicates the precise attribution of herbicide resistance to individual alleles, posing challenges for identifying functional candidates. To overcome this, we focused on triads in which at least one allele was specifically upregulated in R-HN, while the remaining alleles maintained stable expression patterns (Figure 4G).

Differential expression patterns in response to glyphosate between the S-YN and R-HN populations

To further identify NTSR genes associated with glyphosate resistance in *C. rotundus*, the DEGs in response to glyphosate treatment for both biotypes are summarized in supplemental Table 13. In the S-YN population, compared with untreated samples, glyphosate treatment for 12 h induced 8,904 upregulated and 7,644 downregulated genes; at 24 h, 1,432 genes were upregulated and 1,387 downregulated; and at 48 h, 8,930 genes were upregulated and 9,780 downregulated (supplemental Table 15). In the R-HN population, glyphosate treatment for 12 h resulted in 8,447 upregulated and 7,235 downregulated genes; at 24 h, 1,297 genes were upregulated and 1,860 downregulated; and at 48 h, 1,854 genes were upregulated and 2,820 downregulated (supplemental Table 15).

To identify genes responsive to glyphosate, clustering analysis was conducted on gene expression across time points. In both the S-YN and R-HN populations, 15 gene clusters with distinct expression patterns were identified (supplemental Figures 13 and 14; supplemental Table 16). Some clusters exhibited transient upregulation in response to glyphosate, followed by a return to baseline expression (e.g., clusters 1 and 2 in R-HN, clusters 2, 6, and 11 in S-YN), whereas others showed transient downregulation before recovering to high expression levels (e.g., cluster 4 of R-HN), reflecting the dynamic and diverse expression patterns of gene responses to glyphosate (supplemental Figures 13 and 14). Notably, certain gene clusters exhibited a consistent pattern of sustained upregulation or downregulation in response to glyphosate (supplemental Figures 13 and 14). Genes in cluster 14 from the R-HN population and cluster 5 from the S-YN population showed no changes in expression within 24 h but upregulated expression at 48 h (Figure 5A and 5B). In contrast, genes in cluster 5 of the R-HN population and cluster 15 of the S-YN

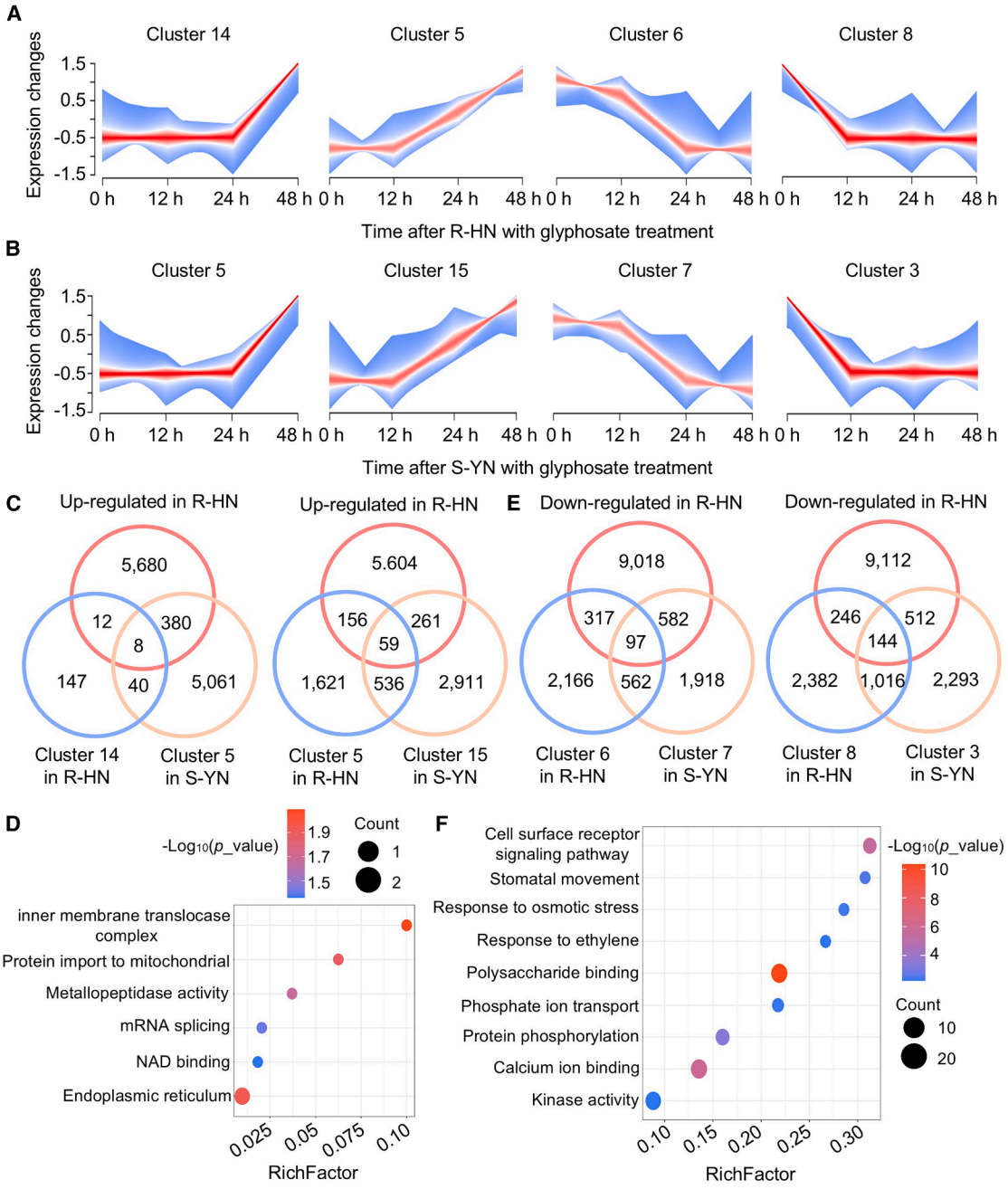

Figure 5. Expression patterns in response to glyphosate in the S-YN and R-HN biotypes.

(A and B) Representative gene expression clusters across different time points in the R-HN **(A)** and S-YN **(B)** populations.

(C) Venn diagrams showing the overlap of upregulated genes among R-HN upregulated genes, cluster 14 of R-HN, and cluster 5 of S-YN (left), and among R-HN upregulated genes, cluster 5 of R-HN, and cluster 15 of S-YN (right).

(D) Functional enrichment of overlapping upregulated genes.

(E) Venn diagrams showing the overlap of downregulated genes among R-HN downregulated genes, cluster 6 of R-HN, and cluster 7 of S-YN (left), and among R-HN downregulated genes, cluster 8 of R-HN, and cluster 3 of S-YN (right).

(F) Functional enrichment of overlapping downregulated genes.

population were upregulated at 12 h post-treatment and continued to exhibit sustained upregulation (Figure 5A and 5B). Conversely, genes in cluster 6 of the R-HN population and cluster 7 of the S-YN population displayed continuous downregulation following glyphosate treatment (Figure 5A and 5B). Additionally, genes in cluster 8 of R-HN and cluster 3 of S-YN were significantly downregulated at 12 h, and their expression levels remained low (Figure 5A and 5B).

Overlapping analysis identified eight genes that were both up-regulated in the R-HN population and exhibited glyphosate-induced upregulation in cluster 14 of R-HN and cluster 5 of

S-YN (Figure 5C). Additionally, 59 upregulated genes in the R-HN population overlapped with those in cluster 5 of R-HN and cluster 15 of S-YN, showing consistent upregulation in response to glyphosate (Figure 5C). Functional enrichment analysis revealed that these overlapping upregulated genes were predominantly associated with biological processes such as mitochondrial protein import via the inner membrane translocase complex, protein import into the mitochondrial matrix, mRNA splicing via the spliceosome, and NAD binding (Figure 5D). Similarly, overlapping analysis identified 241 downregulated genes (97 and 144) that were shared between glyphosate-responsive genes and those downregulated in the R-HN population (Figure 5E); these genes were consistently downregulated in R-HN and also exhibited glyphosate-induced downregulation. Functional enrichment analysis showed that these overlapping genes were significantly enriched in pathways associated with cell surface receptor signaling, stomatal movement, responses to osmotic stress and ethylene, polysaccharide binding, and phosphate ion transport (Figure 5F).

Overexpression of *CrABCG15* and *CrCASPL2C2* confers glyphosate resistance in yeast

Among the 67 upregulated genes in the R-HN population—comprising 8 overlapping genes upregulated in R-HN and 59 genes from clusters continuously upregulated in both R-HN and S-YN—that also responded to glyphosate (Figure 5C), 19 genes exhibited alleles in the R-HN population with either upregulation or stable expression (supplemental Figure 15; supplemental Table 17). Protein annotation revealed that Cro14114, annotated as an ABC transporter G family member 11-like protein (CrABCG11), and Cro57627, annotated as an ABC transporter G family member 15-like protein (CrABCG15), are members of the ABC transporter family that has been previously associated with glyphosate transport resistance (supplemental Table 17). Additional genes identified in this group included a laccase-4-like protein (Cro65458), a MYB-related protein 306-like protein (Cro16399), and CASP-like protein 2C2 (Cro56815; CrCASPL2C2), among others (supplemental Table 17).

Five annotated genes were selected for functional validation. Expression profiling revealed that *CrCASPL2C2* (*Cro56815*) and its allele *Cro57438* were upregulated in the R-HN population, whereas another allele, *Cro57130*, remained stable (Figure 6A). Similarly, *CrABCG15* (*Cro57627*), *CrLAC4* (*Cro65458*), *CrMyb306* (*Cro16399*), and *CrCUT1* (*Cro20542*) were upregulated in R-HN, with no differential expression observed in their alleles (Figure 6A). For functional assessment, heterologous expression was performed in a glyphosate-sensitive yeast strain (W303a). Gene-transformed cells and vector-only control cells were cultured in SG/-Ura medium supplemented with 0–60 mM glyphosate. Results indicated that *Cro16399* and *Cro20542* exhibited growth patterns similar to the GFP control, suggesting no functional role in glyphosate response (Figure 6B). Notably, *CrCASPL2C2* (*Cro56815*)- and *CrABCG15* (*Cro57627*)-transformed cells exhibited enhanced survival compared with GFP controls under 45 and 60 mM glyphosate (Figure 6B and supplemental Figure 16), whereas *Cro65458* (*CrLAC4*) exhibited increased sensitivity under the same conditions (Figure 6B).

Homology modeling and molecular docking were employed to elucidate the structural interactions of the five candidate genes with glyphosate. Three genes met the predefined thresholds, showing strong glyphosate-binding affinity (binding energy < -2 kcal mol^{-1} and sequence identity >30%) (supplemental Table 17). Comparative analysis of the molecular docking results for the three EPSPS alleles (-3.66, -4.60, and -3.97 kcal mol^{-1}) revealed no significant differences in binding affinity (supplemental Figure 17). A randomly selected microtubule-associated protein (Cro36999) was included as a negative control and exhibited a binding energy of -1.96 kcal mol^{-1}, lower than that of EPSPS and the experimentally validated candidate genes. Docking analyses further revealed that glyphosate binds to the active site of the stabilized heme with varying affinities across different proteins. For the glyphosate-resistant protein CrCASPL2C2 (Cro56815), glyphosate exhibited a binding energy of -2.99 kcal mol^{-1}, forming hydrogen bonds with Asn81A, Gln90A, and Ser92A within the binding pocket (Figure 6C). The glyphosate-resistant CrABCG15 (Cro57627) exhibited a binding energy of -3.32 kcal mol^{-1}, with glyphosate forming hydrogen bonds with Gly67A, Ser68A, Gly69A, Lys70A, Ser71A, and Thr72A (Figure 6D). Notably, the strongest glyphosate binding was observed for the increased glyphosate-sensitive protein CrLAC4 (Cro65458), which had a binding energy of -4.95 kcal mol^{-1} and formed hydrogen bonds with Lys70A and Glu171A (Figure 6E). Conversely, the glyphosate-sensitive proteins Cro16399 and Cro20542 exhibited weaker binding affinities, with binding energies of -1.96 and -1.84 kcal mol^{-1}, respectively, falling below the threshold. Collectively, these results suggest that molecular docking is a useful tool for identifying functional glyphosate resistance genes.

DISCUSSION

Here, we present the first triploid chromosome-level assembly of *C. rotundus*, one of the most invasive and economically detrimental weed species, notable for its robust stress tolerance and herbicide resistance (Bendixen and Nandihalli, 1987). Unlike many other weeds, *C. rotundus* is a naturally occurring triploid species with high clonal propagation, which complicates eradication strategies. Beyond its agricultural threat, *C. rotundus* possesses significant medicinal value in traditional Chinese medicine (Srivastava et al., 2013). Its underground tubers are rich in bioactive compounds and are widely used to treat menstrual disorders, digestive issues, and inflammatory diseases (Dang et al., 2011; Kumar et al., 2013; Srivastava et al., 2013; Peerzada et al., 2015). Key constituents, including terpenoids, flavonoids, volatile oils, and alkaloids (El-Kareem and Farouk, 1970; Ghannadi et al., 2012), exhibit antioxidant, antimicrobial, anti-inflammatory, and analgesic properties, underscoring their potential for drug development (Ahmad et al., 2012; Kumar et al., 2013; Rocha et al., 2020; Mohamed et al., 2022). Consequently, this genome assembly provides a valuable genetic resource for future studies on weed biology, herbicide resistance mechanisms, and the medicinal properties of *C. rotundus*.

Weed genomes display remarkable diversity, reflecting the wide phylogenetic distribution of weedy species, which often lack closely related model or crop species for comparative analyses.

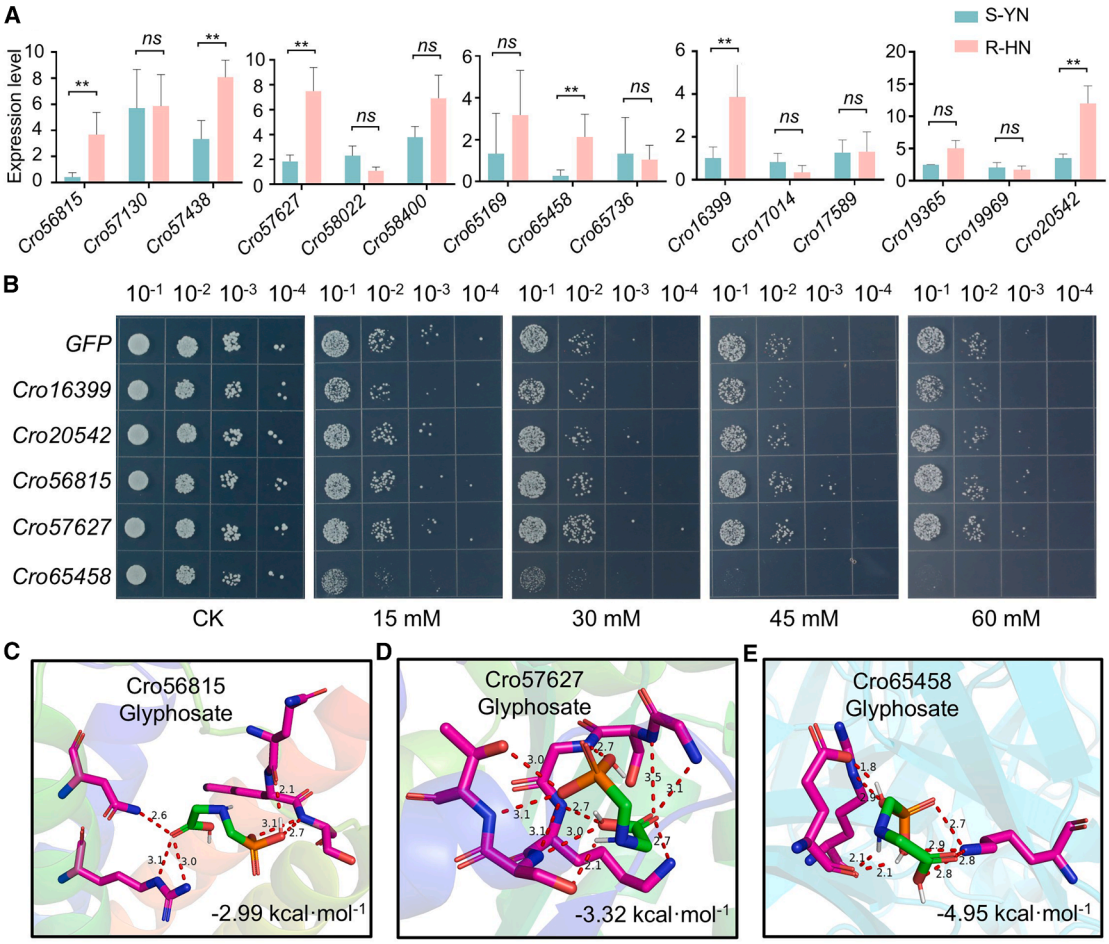

Figure 6. Structure, expression, and functional validation of candidate glyphosate resistance genes.

(A) Expression levels of *Cro56815*, *Cro57627*, *Cro65458*, *Cro16399*, *Cro20542*, and their homoeologs within allelic triads in the S-YN and R-HN populations. **indicate significant differences determined by DESeq2 ($|\log_2(\text{fold change})| \geq 1$ and FDR < 0.05) ns, not significant.

(B) Growth responses of vector-transformed (GFP control) and candidate gene–transformed yeast cells after 2 days of incubation in SG/-Ura medium supplemented with 0, 15, 30, 45, and 60 mM glyphosate, starting from different initial cell densities.

(C–E) Predicted glyphosate binding poses in the active sites of Cro56815 **(C)**, Cro57627 **(D)**, and Cro65458 **(E)**. Heme is shown as orange sticks, protein residues as green sticks, and glyphosate as yellow sticks. Distances between interacting atoms are indicated in Ångströms.

Across all measurable metrics, weed genomes vary considerably in size, complexity, and gene content (Montgomery et al., 2024). Polyploidy is a major driver of plant genome evolution, contributing to structural complexity, gene redundancy, and adaptive potential (Jiao and Paterson, 2014; Van de Peer et al., 2017). To date, 32 weed genomes have been sequenced, predominantly from diploid species (International Wheat Genome Sequencing Consortium [IWGSC], 2018; Sun et al., 2022; Chen et al., 2024b). The *C. rotundus* genome analyzed here is among the most compact triploid plant genomes published to date (875.13 Mb), smaller than triploid *Cavendish banana* (1.42 Gb) (Huang et al., 2023) and triploid poplar (1.07 Gb) (Tong et al., 2022). This compact genome size, combined with high assembly quality, makes *C. rotundus* a promising model for investigating the genomic architecture, haplotype divergence, and allele dosage effects of triploid plants.

Despite its triploid genome structure, *C. rotundus* shows no evidence of recent whole-genome duplication (WGD), as indicated by the absence of a distinct Ks peak and large-scale syntenic blocks (supplemental Figure 18). This contrasts with many polyploid crops and weeds, including decaploid *Houttuynia cordata* (Huang et al., 2024), tetraploid *L. chinensis* (Wang et al., 2022), and allotetraploid *Cynodon dactylon* (Wang et al., 2024), in which WGD has driven adaptive evolution. WGD-associated genome repatterning is widely recognized for promoting functional innovation and stress resilience through gene dosage effects, sub-functionalization, and neofunctionalization (Adams and Wendel, 2005; Murat et al., 2010). In contrast, *C. rotundus* may have evolved primarily through small-scale duplications and structural variants, with its clonal propagation strategy potentially buffering against genomic instability and reducing the necessity for large-scale duplication events.

Genomic studies have markedly enhanced our understanding of weed adaptations to environmental biotic and abiotic stresses. A notable trait associated with environmental adaptation in weeds is herbicide resistance (Gaines et al., 2020). Comparative genomics involving herbicide-susceptible and resistant

individuals from the same species, as well as across species, can provide insights into innovations in herbicide resistance pathways (Kreiner et al., 2018). In this study, dose-response assays revealed that despite no prior exposure to glyphosate or glufosinate, the S-YN population exhibited GR_{50} values of 3603.86 and 909.70 g a.i./ha, respectively, surpassing recommended field rates and suggesting inherent resistance to both herbicides. These findings suggest that, even in the absence of direct herbicide selection pressure, *C. rotundus* populations may harbor a baseline tolerance to commonly used herbicides. In polyploids, NTSR may be reinforced by subgenome specialization or homoeologous buffering, enhancing adaptability to herbicide stress (Chen et al., 2023). Triploidy provides genomic redundancy, buffering the deleterious effects of herbicides by maintaining multiple functional gene copies, thus mitigating the impact of target-site mutations or enzymatic inhibition. Polyploid genomes also exhibit enhanced transcriptional plasticity, facilitating rapid activation of antioxidant and xenobiotic metabolism under chemical stress. Moreover, as a C_4 species, *C. rotundus* possesses a highly efficient carbon fixation system that reduces photorespiration and limits oxidative damage, potentially improving tolerance to reactive oxygen species generated during glyphosate treatment (Monson and Rawsthorne, 2000). Collectively, the triploid genome architecture, C_4 metabolic advantages, and NTSR mechanisms may underpin a baseline tolerance to glyphosate. However, the relative contributions of these mechanisms remain to be elucidated. Among six populations sampled across China, only the R-HN population exhibited dual resistance to glyphosate and glufosinate compared with the S-YN population. Transcriptome profiling and expression dynamics of homoeologous triads revealed significant differences in gene expression between S-YN and R-HN even in the absence of herbicide treatment. Specifically, 1,200 triads were uniquely expressed in S-YN, predominantly associated with growth and developmental processes, whereas 688 triads were uniquely upregulated in R-HN, associated with stress responses, particularly herbicide resistance. Furthermore, triads expressed in both populations exhibited significantly higher transposable element (TE) enrichment within gene bodies than the other categories (supplemental Figure 19). However, when both gene body and promoter regions were considered, no significant differences in TE enrichment were observed (supplemental Figure 19). Additionally, the S-YN population exhibited a more balanced expression of homoeologous triads, whereas the R-HN population showed pronounced expression divergence, likely reflecting herbicide-driven selection.

The genomic data of *C. rotundus* provide an important opportunity to examine variation associated with TSR and enable the discovery of NTSR genes. *GS2* genes, including *Cro69233*, were significantly upregulated in the R-HN population, which displayed strong glufosinate resistance. This finding aligns with those in *Amaranthus palmeri*, where *GS2* overexpression confers resistance to glufosinate (Noguera et al., 2022). In contrast, glyphosate resistance in *C. rotundus* appears to be dominated by NTSR mechanisms. By integrating transcriptomic profiles across multiple time points after glyphosate exposure with molecular docking and yeast-based functional assays, we identified two candidate NTSR genes, *CrABCG15* and *CrCASPL2C2*. Both genes exhibited glyphosate-binding affinity and conferred glyphosate resistance in heterologous systems, confirming their functional relevance. *CrABCG15* encodes an ABC transporter that likely facilitates glyphosate efflux or sequestration, thereby limiting its interaction with EPSPS, similar to *EcABCC8* in glyphosate-resistant *Echinochloa colona*, which actively exports glyphosate (Pan et al., 2021). *CrCASPL2C2* is a member of the CASP-like (CASPL) family and may participate in cellular compartmentalization or stress signaling through its membrane-associated domain (Barbosa et al., 2019). Given that *CASPLs* are commonly induced under abiotic stress conditions such as cold, salt, and drought (Yang et al., 2015; Su et al., 2023; Chen et al., 2025), these findings suggest that they play crucial roles in environmental stress adaptation and may also mediate responses to herbicide-induced stress.

In summary, this study presents a chromosome-level genome assembly of triploid *C. rotundus*, offering new insights into its evolutionary history and herbicide resistance mechanisms. Population-level analyses revealed both TSR and NTSR to glufosinate and glyphosate, including GS gene amplification and functional validation of the glyphosate-related candidates *CrABCG15* and *CrCASPL2C2*. Collectively, these findings enhance our understanding of the genetic basis of herbicide resistance in *C. rotundus*. Furthermore, the *C. rotundus* reference genome represents a valuable resource for advancing weed evolutionary biology, elucidating crop–weed interactions, and informing innovative weed management strategies under future climate change scenarios.

METHODS

C. rotundus plants and materials

The genome-sequenced *C. rotundus* population (NCBI Taxonomy ID: 512623) was collected from an industrial hemp (*Cannabis sativa*) field in Xishuangbanna, Yunnan Province (21.98°N, 100.41°E), where neither glyphosate nor glufosinate had been applied. This population was designated S-YN. Tubers from S-YN were propagated and grown under controlled conditions (28 °C, continuous darkness) in a growth chamber until reaching the four- to five-leaf stage, at which point aboveground tissues were harvested for genomic DNA extraction and sequencing.

Five additional *C. rotundus* populations were collected from agricultural sites across China and designated as HN, CS, HB, HeN, and ZJ. Specifically, HN (Changde, Hunan, 28.86°N, 111.94°E) was collected from vegetable fields (*Brassica oleracea*, *Benincasa hispida*); CS (Changsha, Hunan, 28.20°N, 113.08°E) from urban green spaces (lawns); HB (Xianning, Hubei, 29.91°N, 114.17°E) from vegetable fields (*Zea mays*, *Ipomoea batatas*); HeN (Xinyang, Henan, 32.08°N, 110.00°E) from maize fields; and ZJ (Xiaoshan, Zhejiang, 33.53°N, 120.44°E) from rice paddies. Tubers from all populations were cultivated under natural summer conditions in a greenhouse in Changsha and grown to the four- to five-leaf stage for herbicide (glyphosate and glufosinate) resistance assessment using a 3WP-2000 track sprayer. For each herbicide concentration, four to five tubers were used, with three independent biological replicates included in all experiments.

Additionally, plants from the S-YN and HN populations (designated as R-HN) at the four- to five-leaf stage were treated with glyphosate (2,700 g a.i./ha) using the 3WP-2000 track sprayer. Top leaves were collected at 12, 24, and 48 h post-treatment, flash-frozen in liquid nitrogen, and stored at −80°C. RNA was extracted from three biological replicates per time point, each consisting of at least five individual plants, and subsequently subjected to RNA-seq.

DNA extraction and sequencing

High-quality genomic DNA was extracted from mixed tissues using the cetyltrimethylammonium bromide (CTAB) method, followed by RNase A treatment to eliminate RNA contaminants. DNA quality and concentration were assessed using a NanoDrop 2000 spectrophotometer (NanoDrop Technologies, Wilmington, DE), and DNA integrity was evaluated through 0.8% agarose gel electrophoresis.

For long-read sequencing, a SMRTbell library was prepared using the SMRTbell Express Template Prep Kit 2.0. Approximately 15 μg of genomic DNA was sheared into ~15 kb fragments using a Covaris g-TUBE. Fragment size distribution was analyzed with the Femto Pulse system, and large fragments (> 15 kb) were selectively enriched using the BluePippin size-selection system (Sage Science). Library quality and concentration were quantified using the Femto Pulse and a Qubit fluorometer (Life Technologies), respectively. Sequencing was performed on a PacBio Sequel II system using 8M SMRT cells (Pacific Biosciences) at Frasergen Bioinformatics (Wuhan, China). For short-read sequencing, a paired-end Illumina library with a 350 bp insert size was constructed using the Illumina Genomic DNA Sample Preparation Kit, following the manufacturer's instructions.

RNA extraction, library preparation, and sequencing

Total RNA was extracted using TRIzol reagent, and RNA purity and integrity were assessed using a NanoDrop 2000 spectrophotometer and a Bioanalyzer 2100. RNA quality was further confirmed through 1.5% agarose gel electrophoresis. mRNA was enriched using poly-T oligo-attached magnetic beads, followed by library construction with the VAHTS Universal V6 RNA-seq Library Kit for MGI, incorporating unique sample indices. Library concentration and fragment size distribution were quantified using a Qubit 3.0 Fluorometer and a Bioanalyzer 2100. Sequencing was carried out on the MGI-SEQ 2000 platform at Frasergen Bioinformatics (Wuhan, China) according to standard protocols.

Genome assembly with HiFi reads and Hi-C data

High-accuracy HiFi reads were generated using three SMRT cells on the PacBio Sequel II/Revio platform. Genome assembly was performed using HiFiasm (v0.19.5) (Cheng et al., 2021) with default parameters, and sequence graphs were converted from GFA to FASTA format using gfatools. For chromosome-level scaffolding, Hi-C reads were trimmed using Trimmomatic (v0.40) to remove adapters and low-quality bases and subsequently aligned to contigs with Juicer (v1.6) to calculate contact frequency. Mis-assemblies were corrected through two iterative rounds of 3D-DNA (v180922) with default parameters. The resulting scaffolds were further refined and manually curated with Juicebox Assembly Tools (v1.11.08) to correct mis-joins and resolve heterozygosity, producing a high-contiguity chromosome-scale genome assembly. Homologous chromosomes were distinguished based on well-resolved Hi-C interaction signals and were subsequently assigned randomly to the three haplomes.

Auality assessment of the assembly

To comprehensively evaluate the quality of the *C. rotundus* genome assembly, HiFi reads were mapped using BWA and Minimap2 (v2.21) (Li, 2018) with the parameters "-ax map-ont/map-hifi" to assess coverage and completeness. K-mer-based quality assessment (k = 19 bp) was performed using the Merqury pipeline (v1.3) with HiFi reads. Assembly completeness was evaluated with BUSCO v3.0.2 (Seppey et al., 2019) using the embryophyta_odb10 dataset. Additionally, the LTR assembly index was calculated to assess the completeness of complex repetitive sequences.

Genome annotation

Repetitive sequences were predicted using two complementary approaches. Homology-based detection involved aligning the genome with the RepBase database (http://www.girinst.org/repbase) (Jurka et al., 2005) using RepeatMasker (v4.1.2) (Smit et al., 1996) and RepeatProteinMask (revision 1.36) (Smit et al., 1996) to identify sequences homologous to known repeats. For de novo prediction, a custom repeat library was generated using RepeatModeler (v2.0.1) and LTR-FINDER (v1.0.7) (Xu and Wang, 2007), followed by annotation with RepeatMasker. Tandem repeats were identified and refined using TRF (v4.09.1) (Price et al., 2005).

Gene annotation integrated homology-based, transcriptome-based, and ab initio predictions. For homology-based annotation, protein sequences from closely related plant species were aligned using tblastn (v2.11.0+), followed by structural refinement with Exonerate (v2.4.0) (Slater and Birney, 2005). Transcriptome-based prediction integrated RNA-seq and Iso-Seq data aligned to the genome using PASA (v2.4.1) (Haas et al., 2003) to refine splice sites and exon boundaries. De novo prediction utilized probabilistic models (e.g., codon usage, exon–intron distributions) in Augustus (v3.4.0) (Stanke et al., 2006), GlimmerHMM (v3.0.4) (Majoros et al., 2004), and other tools, which had limited accuracy for UTR and splice site identification. All predictions were integrated into a non-redundant gene set using MAKER (v3.01.03) (Holt and Yandell, 2011), with structural refinement conducted using PASA (Haas et al., 2003). Functional annotation was performed by aligning predicted proteins with Swiss-Prot (Bairoch and Apweiler, 2000), NR, PFAM (Mistry et al., 2021), GO (Ashburner et al., 2000), KEGG (Kanehisa and Goto, 2000), InterPro (Blum et al., 2021), and TrEMBL (O'Donovan et al., 2002).

tRNA sequences in the genome were identified using tRNAscan-SE (v2.0.9) (Lowe and Eddy, 1997), based on structural features. rRNA sequences were predicted using RNAmmer (v1.2). miRNA and snRNA sequences were predicted using the covariance models from the Rfam database (http://xfam.org/) (Griffiths-Jones et al., 2005) with INFERNAL (v1.1.4) software (Nawrocki and Eddy, 2013).

Gene family clustering and phylogenetic analysis

Orthologous gene families were clustered using OrthoFinder2 (v2.5.4) (Emms and Kelly, 2019) to assess sequence similarity across species, including the outgroup *Arabidopsis thaliana* and closely related species such as *Cyperus esculentus*, *Rhynchospora breviuscula*, *Carex cristatella*, and *Carex littledalei*. Additional species included *Oryza sativa*, *Zea mays*, *Sorghum bicolor*, *Setaria italica*, *Eleusine indica*, and *Leptochloa chinensis*. Gene sets were preprocessed to retain only the longest coding isoform per gene to reduce redundancy. Protein sequences were pairwise aligned using DIAMOND (Buchfink et al., 2015) to obtain similarity relationships among the protein sequences of all species. OrthoFinder2 clustered orthogroups based on these alignments, distinguishing single-copy from multi-copy orthogroups. Single-copy orthologs are defined as those having exactly one gene copy in all species, while multi-copy orthologs arise from extensive gene duplication throughout evolution. For phylogenetic reconstruction, single-copy orthologs with protein lengths ≥100 amino acids were retained. Multiple sequence alignments for each orthogroup were generated using MUSCLE (v3.8.31) (Edgar, 2004), concatenated into a supergene alignment in PHYLIP format, and then subjected to maximum likelihood tree construction using RAxML (v8.2.12) (Stamatakis, 2014). Divergence times were estimated using r8s (v1.81) (Sanderson, 2003) and the mcmctree module in PAML (v4.10.0) (Yang, 1997), calibrated with fossil or molecular time points from TimeTree (Hedges et al., 2006) and relevant literature.

Gene family expansion and contraction, and positive selection analysis

Gene family expansion and contraction were analyzed using CAFE (v4.2.1) (De Bie et al., 2006) based on orthogroup clustering. Gene family expansion and contraction indicate gene gain and gene loss during evolution, respectively. Positive selection was evaluated using Ka/Ks analysis, where Ka/Ks > 1 indicates positive selection. For single-copy orthologs identified through clustering analysis, lineage-specific

positive selection was further examined using branch-site models implemented in PAML (v4.10.0) (Yang, 1997). Positively selected genes and significantly expanded or contracted gene families were subjected to GO and KEGG enrichment analyses with FDR correction (q value <0.05) (Ashburner et al., 2000; Kanehisa and Goto, 2000).

Gene expression quantification and differential expression analysis

Raw sequencing reads were quality-filtered using SOAPnuke (v2.1.0) (Chen et al., 2018) with the following parameters: "lowQual = 20, nRate = 0.005, and qualRate = 0.5". The filtering procedure sequentially removed adapter-contaminated reads, discarded paired-end reads containing > 0.5% undetermined (N) bases, and excluded reads where >50% of bases had QPhred scores ≤20. Clean reads were aligned to the *C. rotundus* reference genome using Bowtie2 (v2.3.5) (Langmead, 2010) with default parameters. Gene expression levels were quantified using RSEM (v1.3.3) (Li and Dewey, 2011) and normalized to FPKM. Differential expression analysis was performed on read counts normalized for sequencing depth using DESeq2 (v1.22.2) (Trapnell et al., 2010), applying a significance threshold of $|\log_2(\text{fold change})| \geq 1$ and FDR < 0.05. Genes from four time points during glyphosate treatment were clustered using the fuzzy c-means algorithm implemented in the Mfuzz package (v2.64.0) in R (Kumar and E Futschik, 2007).

Allele identification and homoeolog expression patterns in haplotypes

To identify alleles in the *C. rotundus* genome, DIAMOND (v2.0.15) (Buchfink et al., 2021) was used to align protein sequences across three haploid assemblies, classifying alleles into three categories: a 1:1:1 correspondence, pairs of alleles, and the remaining based on identity scores. Homoeolog expression patterns were analyzed using gene expression data from herbicide-untreated samples of the S-YN and R-HN populations, focusing on gene triads exhibiting a 1:1:1 correspondence. A homoeolog was considered expressed if its FPKM value exceeded 0.5 in either population. Relative expression levels of hapI, hapII, and hapIII homoeologs were standardized following established methods (Ramirez-Gonzalez et al., 2018; Huang et al., 2023) using the formula: Expression_hapX = FPKM (hapX)/(FPKM (hapI) + FPKM (hapII) + FPKM (hapIII)), where X represents I, II, or III. Relative expression levels for each triad were visualized using ternary plots generated with the R package ggtern (v3.5.0) (Hamilton and Ferry, 2018). Homoeolog expression bias was classified into seven categories: one balanced group (with similar expression across all three homoeologs) and six biased groups in which a single homoeolog was either dominant or suppressed relative to the others.

EPSPS and *GS* gene analysis

Protein sequences of rice *EPSPS* (*LOC_Os06g04280*) and *GS2* (*LOC_Os10g31820*) were aligned to *C. rotundus* protein sequences using BLASTp (Camacho et al., 2009), retaining hits with ≥50% coverage. Additionally, the coding sequences of *C. rotundus EPSPS* and *GS* homologs were aligned to the *C. rotundus* genome to identify homologous genes (Camacho et al., 2009). To examine target-site mutations, nucleotide variations within specific *EPSPS and GS2 regions were visualized using the* Integrative Genomics Viewer (Thorvaldsdottir et al., 2013) based on BAM files from the R-HN and S-YN populations.

Homology modeling and molecular docking

Homology modeling of candidate proteins was performed using SWISS-MODEL (Waterhouse et al., 2018), selecting templates with ≥30% sequence identity and optimizing structures based on GMQE (0–1 scale) and QMEAN (−4 to 0) scores. Molecular docking was performed using AutoDock Tools v1.5.6 with a semiflexible docking approach. Receptor proteins were prepared by adding hydrogen atoms and optimizing charges, while ligands (glyphosate retrieved from PubChem: https://pubchem.ncbi.nlm.nih.gov/) were assigned rotatable bonds and energy-minimized using Chem3D. Docking grids were defined using AutoGrid 4, and ligand binding was assessed using the Lamarckian genetic algorithm (20 runs per ligand). Blind docking was applied to examine glyphosate interactions. Binding conformations were visualized using PyMOL v2.3.0, and docking results were evaluated based on empirical binding energy scores and spatial complementarity.

RT-qPCR and genomic DNA-based qPCR for *GS2* genes

Genomic DNA was extracted from samples of the S-YN and R-HN populations using the CTAB method, and total RNA was isolated from the same material as described above. RNA was reverse-transcribed into complementary DNA using the HiScript II Q RT SuperMix (Vazyme, Nanjing, China) according to the manufacturer's protocol. Primers for genomic DNA–based qPCR were designed to span exons and introns, whereas RT–qPCR primers were designed using the IDT online tool (https://sg.idtdna.com/scitools/Applications/RealTimePCR/) (supplemental Table 18). qPCR assays were performed with three biological replicates and three technical replicates. *Actin* served as the reference gene for normalization in both genomic DNA-based qPCR and RT-qPCR analyses (Noguera et al., 2022). Relative expression levels were calculated using the $2^{-\Delta\Delta Ct}$ method.

Genetic transformation of candidate genes in yeast cells

Gene-specific primers were designed to amplify the full-length complementary DNA of candidate glyphosate-resistance genes, including *Cro16399*, *Cro20542*, *Cro56815*, *Cro57627*, and *Cro65458*. Purified PCR products were cloned into pYES2 vectors linearized with *Kpn*I/*Eco*RI (NEB) digestion using In-Fusion assembly (TaKaRa, Japan). Verified recombinant vectors were transformed into the glyphosate-sensitive yeast strain W303a using the PEG/LiAc method. Positive colonies selected from SD/Ura plates (PM2271; Coolaber, Beijing) after 48 h of incubation were PCR-validated and cultured to mid-log phase ($1–2 \times 10^7$ cells ml^{-1}). Serial dilutions ($10^3–10^7$ cells ml^{-1}) were spotted onto SG/Ura agar plates (PM22725; Coolaber) containing 0–60 mM glyphosate. W303a transformed with an empty vector served as the negative control. Phenotypic comparisons were performed after 72 h of growth at 30°C.

DATA AND CODE AVAILABILITY

The genome reference sequence files generated in this study have been deposited in the Genome Warehouse (GWH) of the National Genomics Data Center (NGDC) under accession number GWHGDIW00000000.1. The raw sequencing reads have been submitted to the Genome Sequence Archive (GSA) under accession number CRA024621 (Wu et al., 2025). Both datasets are publicly accessible at https://ngdc.cncb.ac.cn.

FUNDING

This work was supported by the earmarked fund for China Agricultural Research System (CARS-16-E19), the Foundation for Tobacco Science of China National Tobacco Corporation (110202401015, LS-05), the National Key Research and Development Program of China (2023YFD1400504), the Modern Agricultural Industrial Technology System of Hunan Province (grant no. 2022–31), and the Yuelushan Laboratory Breeding Program (YLS-2025-ZY03010).

ACKNOWLEDGMENTS

No conflict of interest declared.

AUTHOR CONTRIBUTIONS

L.P., Z.L., and L.B. designed and supervised the study. Z.L. performed the bioinformatic analyses with assistance from Y.L. and S.Z. Plants were grown, phenotyped, harvested, and submitted for sequencing by L.W., with assistance from M.L., H.C., J.H., and L.Y. J.L. and S.H. performed the experiments. Z.L. wrote the manuscript and L.P reviewed and edited the manuscript.

SUPPLEMENTAL INFORMATION

Supplemental information is available at *Plant Communications Online*.

Received: June 5, 2025
Revised: September 13, 2025
Accepted: November 21, 2025
Published: November 26, 2025

REFERENCES

Adams, K.L., and Wendel, J.F. (2005). Polyploidy and genome evolution in plants. Curr. Opin. Plant Biol. **8**:135–141.

Agahiu, A. (2020). Assessment of some herbicides for the control of purple nutsedge (Cyperus rotundus) in soybean (Glycine max (L.) Merrill). GSC Biol. Pharm. Sci. **12**:229–234.

Ahmad, M., Mahayrookh, M., Rehman, A.B., and Jahan, N. (2012). Analgesic, antimicrobial and cytotoxic effect of Cyperus rotundus ethanol extract. Pak J Pharmacol **29**:7–13.

Ashburner, M., Ball, C.A., Blake, J.A., Botstein, D., Butler, H., Cherry, J.M., Davis, A.P., Dolinski, K., Dwight, S.S., Eppig, J.T., et al. (2000). Gene ontology: tool for the unification of biology. The Gene Ontology Consortium. Nat. Genet. **25**:25–29.

Atwell, B., Thomson, C., Greenway, H., Ward, G., and Waters, I. (1985). A study of the impaired growth of roots of Zea mays seedlings at low oxygen concentrations. Plant Cell Environ. **8**:179–188.

Avila-Garcia, W.V., Sanchez-Olguin, E., Hulting, A.G., and Mallory-Smith, C. (2012). Target-site mutation associated with glufosinate resistance in Italian ryegrass (Lolium perenne L. ssp. multiflorum). Pest Manag. Sci. **68**:1248–1254.

Bairoch, A., and Apweiler, R. (2000). The SWISS-PROT protein sequence database and its supplement TrEMBL in 2000. Nucleic Acids Res. **28**:45–48.

Barbosa, I.C.R., Rojas-Murcia, N., and Geldner, N. (2019). The Casparian strip-one ring to bring cell biology to lignification? Curr. Opin. Biotechnol. **56**:121–129.

Bendixen, L.E., and Nandihalli, U.B. (1987). Worldwide distribution of purple and yellow nutsedge (Cyperus rotundus and C. esculentus). Weed Technol. **1**:61–65.

Blum, M., Chang, H.Y., Chuguransky, S., Grego, T., Kandasaamy, S., Mitchell, A., Nuka, G., Paysan-Lafosse, T., Qureshi, M., Raj, S., et al. (2021). The InterPro protein families and domains database: 20 years on. Nucleic Acids Res. **49**:D344–D354.

Buchfink, B., Xie, C., and Huson, D.H. (2015). Fast and sensitive protein alignment using DIAMOND. Nat. Methods **12**:59–60.

Buchfink, B., Reuter, K., and Drost, H.G. (2021). Sensitive protein alignments at tree-of-life scale using DIAMOND. Nat. Methods **18**:366–368.

Camacho, C., Coulouris, G., Avagyan, V., Ma, N., Papadopoulos, J., Bealer, K., and Madden, T.L. (2009). BLAST+: architecture and applications. BMC Bioinf. **10**:421.

Carvalho-Moore, P., Norsworthy, J.K., González-Torralva, F., Hwang, J.-I., Patel, J.D., Barber, L.T., Butts, T.R., and McElroy, J.S. (2022). Unraveling the mechanism of resistance in a glufosinate-resistant Palmer amaranth (Amaranthus palmeri) accession. Weed Sci. **70**:370–379.

Carvalho-Moore, P., Borgato, E.A., Cutti, L., Porri, A., Meiners, I., Lerchl, J., Norsworthy, J.K., and Patterson, E.L. (2025). A rearranged Amaranthus palmeri extrachromosomal circular DNA confers resistance to glyphosate and glufosinate. Plant Cell **37**:koaf069.

Chand, M., Singh, S., Bir, D., Singh, N., and Kumar, V. (2013). Halosulfuron Methyl: A New Post Emergence Herbicide in India for Effective Control of Cyperus rotundus in Sugarcane and Its Residual Effects on the Succeeding Crops. Sugar Tech **16**:67–74.

Charles, G.W. (1995). Nutgrass (Cyperus rotundus L.) control in cotton (Gossypium hirsutum L.). Aust. J. Exp. Agric. **35**:633–639.

Chauhan, B.S., and Opeña, J. (2012). Growth of purple nutsedge (Cyperus rotundus) in response to interference with direct-seeded rice. Weed Technol. **26**:506–509.

Chen, J., Huang, H., Zhang, C., Wei, S., Huang, Z., Chen, J., and Wang, X. (2015). Mutations and amplification of EPSPS gene confer resistance to glyphosate in goosegrass (Eleusine indica). Planta **242**:859–868.

Chen, J., Shan, B., Li, Z., Chen, Q., Yu, H., Cui, H., and Li, X. (2024a). Unraveling the mechanisms of multiple resistance across glyphosate and glufosinate in Eleusine indica. Pestic. Biochem. Physiol. **206**:106181.

Chen, K., Yang, H., Wu, D., Peng, Y., Lian, L., Bai, L., and Wang, L. (2024b). Weed biology and management in the multi-omics era: progress and perspectives. Plant Commun. **5**:100816.

Chen, K., Yang, H., Peng, Y., Liu, D., Zhang, J., Zhao, Z., Wu, L., Lin, T., Bai, L., and Wang, L. (2023). Genomic analyses provide insights into the polyploidization-driven herbicide adaptation in Leptochloa weeds. Plant Biotechnol. J. **21**:1642–1658.

Chen, Y., Wang, C., Tian, S., Yao, L., Zhu, N., Yang, X., Bai, Z., Liu, L., Zhang, Y., Sun, H., et al. (2025). Abscisic Acid and Ethylene Antagonistically Regulate Root Endodermal Suberization to Mitigate Nonuniform Salt Stress in Cotton. Plant Cell Environ. **48**:3199–3216.

Chen, Y., Chen, Y., Shi, C., Huang, Z., Zhang, Y., Li, S., Li, Y., Ye, J., Yu, C., Li, Z., et al. (2018). SOAPnuke: a MapReduce acceleration-supported software for integrated quality control and preprocessing of high-throughput sequencing data. GigaScienceGigaScience **7**:1–6.

Cheng, H., Concepcion, G.T., Feng, X., Zhang, H., and Li, H. (2021). Haplotype-resolved de novo assembly using phased assembly graphs with hifiasm. Nat. Methods **18**:170–175.

Comont, D., MacGregor, D.R., Crook, L., Hull, R., Nguyen, L., Freckleton, R.P., Childs, D.Z., and Neve, P. (2022). Dissecting weed adaptation: Fitness and trait correlations in herbicide-resistant Alopecurus myosuroides. Pest Manag. Sci. **78**:3039–3050.

Consortium, R.E.X. (2013). Heterogeneity of selection and the evolution of resistance. Trends Ecol. Evol. **28**:110–118.

Cui, L., Sun, Y., Xiao, K., Wan, L., Zhong, J., Liu, Y., Xie, Q., and Zhou, S. (2022). Analysis on the abnormal chromosomal behaviour and the partial female fertility of allotriploid Lilium–'Triumphator'(LLO) is not exceptional to the hypothesis of lily interploid hybridizations. Sci. Hortic. **293**:110746.

DaiYin, C., Dilkes, B., Luo, H., Douglas, A., Yakubova, E., Lahner, B., and Salt, D. (2013). Polyploids exhibit higher potassium uptake and salinity tolerance in Arabidopsis. Science (New York, N.Y.) **341**:658–659.

Dang, G.K., Parekar, R.R., Kamat, S.K., Scindia, A.M., and Rege, N.N. (2011). Antiinflammatory activity of Phyllanthus emblica, Plumbago zeylanica and Cyperus rotundus in acute models of inflammation. Phytother Res. **25**:904–908.

De Bie, T., Cristianini, N., Demuth, J.P., and Hahn, M.W. (2006). CAFE: a computational tool for the study of gene family evolution. Bioinformatics **22**:1269–1271.

Delye, C., Gardin, J., Boucansaud, K., Chauvel, B., and Petit, C. (2011). Non-target-site-based resistance should be the centre of attention for herbicide resistance research: Alopecurus myosuroides as an illustration. Weed Res. **51**:433–437.

Dimaano, N.G., Yamaguchi, T., Fukunishi, K., Tominaga, T., and Iwakami, S. (2020). Functional characterization of cytochrome P450

CYP81A subfamily to disclose the pattern of cross-resistance in Echinochloa phyllopogon. Plant Mol. Biol. **102**:403–416.

Edgar, R.C. (2004). MUSCLE: multiple sequence alignment with high accuracy and high throughput. Nucleic Acids Res. **32**:1792–1797.

Edwards, J.W., and Coruzzi, G.M. (1989). Photorespiration and light act in concert to regulate the expression of the nuclear gene for chloroplast glutamine synthetase. Plant Cell **1**:241–248.

EL-KAREAM, A., and FAROUK, G. (1970). Role of Cyperus rotundus oil in decreasing hair growth. Journal of Complementary Medicine Research **1**:111.

Emms, D.M., and Kelly, S. (2019). OrthoFinder: phylogenetic orthology inference for comparative genomics. Genome Biol. **20**:238.

Freeling, M., Scanlon, M.J., and Fowler, J.E. (2015). Fractionation and subfunctionalization following genome duplications: mechanisms that drive gene content and their consequences. Curr. Opin. Genet. Dev. **35**:110–118.

Gaines, T.A., Patterson, E.L., and Neve, P. (2019). Molecular mechanisms of adaptive evolution revealed by global selection for glyphosate resistance. New Phytol. **223**:1770–1775.

Gaines, T.A., Duke, S.O., Morran, S., Rigon, C.A.G., Tranel, P.J., Küpper, A., and Dayan, F.E. (2020). Mechanisms of evolved herbicide resistance. J. Biol. Chem. **295**:10307–10330.

Ghannadi, A., Rabbani, M., Ghaemmaghami, L., and Malekian, N. (2012). Phytochemical screening and essential oil analysis of one of the Persian sedges; Cyperus rotundus L. Int. J. Pharmaceut. Sci. Res.Res. **3**:424.

Griffiths-Jones, S., Moxon, S., Marshall, M., Khanna, A., Eddy, S.R., and Bateman, A. (2005). Rfam: annotating non-coding RNAs in complete genomes. Nucleic Acids Res. **33**:D121–D124.

Guo, L., Qiu, J., Ye, C., Jin, G., Mao, L., Zhang, H., Yang, X., Peng, Q., Wang, Y., Jia, L., et al. (2017). Echinochloa crus-galli genome analysis provides insight into its adaptation and invasiveness as a weed. Nat. Commun. **8**:1031.

Gupta, S., Harkess, A., Soble, A., Van Etten, M., Leebens-Mack, J., and Baucom, R.S. (2023). Interchromosomal linkage disequilibrium and linked fitness cost loci associated with selection for herbicide resistance. New Phytol. **238**:1263–1277.

Haas, B.J., Delcher, A.L., Mount, S.M., Wortman, J.R., Smith, R.K., Jr., Hannick, L.I., Maiti, R., Ronning, C.M., Rusch, D.B., Town, C.D., et al. (2003). Improving the Arabidopsis genome annotation using maximal transcript alignment assemblies. Nucleic Acids Res. **31**:5654–5666.

Hamilton, N.E., and Ferry, M. (2018). ggtern: Ternary Diagrams Using ggplot2. J. Stat. Softw. **87**:1–17.

Han, H., Yu, Q., Beffa, R., González, S., Maiwald, F., Wang, J., and Powles, S.B. (2021). Cytochrome P450 CYP81A10v7 in Lolium rigidum confers metabolic resistance to herbicides across at least five modes of action. Plant J. **105**:79–92.

He, S., Tian, J., Ouyang, Y., Liao, Y., Yu, Q., Bai, L., and Pan, L. (2024). Glyphosate Resistance in Eleusine indica: Involvement of CYP71AK44 in Addition to EPSPS Gene Overexpression. J. Agric. Food Chem. **72**:23758–23765.

Hedges, S.B., Dudley, J., and Kumar, S. (2006). TimeTree: a public knowledge-base of divergence times among organisms. Bioinformatics **22**:2971–2972.

Hollander, H., and Amrhein, N. (1980). The Site of the Inhibition of the Shikimate Pathway by Glyphosate: I. INHIBITION BY GLYPHOSATE OF PHENYLPROPANOID SYNTHESIS IN BUCKWHEAT (FAGOPYRUM ESCULENTUM MOENCH). Plant Physiol **66**:823–829.

Holt, C., and Yandell, M. (2011). MAKER2: an annotation pipeline and genome-database management tool for second-generation genome projects. BMC Bioinf. **12**:491.

Huang, H.R., Liu, X., Arshad, R., Wang, X., Li, W.M., Zhou, Y., and Ge, X.J. (2023). Telomere-to-telomere haplotype-resolved reference genome reveals subgenome divergence and disease resistance in triploid Cavendish banana. Hortic. Res. **10**:uhad153.

Huang, P., Li, Z., Wang, H., Huang, J., Tan, G., Fu, Y., Liu, X., Zheng, S., Xu, P., Sun, M., et al. (2024). A genome assembly of decaploid Houttuynia cordata provides insights into the evolution of Houttuynia and the biosynthesis of alkaloids. Hortic. Res. **11**:uhae203.

International Wheat Genome Sequencing Consortium IWGSC. (2018). Shifting the limits in wheat research and breeding using a fully annotated reference genome. Science **361**:eaar7191.

Jiao, Y., and Paterson, A.H. (2014). Polyploidy-associated genome modifications during land plant evolution. Philos. Trans. R. Soc. Lond. B Biol. Sci. **369**:20130355.

Johnson, N.A., Lemas, J., Montgomery, J., Gaines, T., and Patterson, E. (2025). Genomic structural variation and herbicide resistance. Can. J. Plant Sci. **105**:1–10.

Jurka, J., Kapitonov, V.V., Pavlicek, A., Klonowski, P., Kohany, O., and Walichiewicz, J. (2005). Repbase Update, a database of eukaryotic repetitive elements. Cytogenet. Genome Res. **110**:462–467.

Kanehisa, M., and Goto, S. (2000). KEGG: kyoto encyclopedia of genes and genomes. Nucleic Acids Res. **28**:27–30.

Kasianov, A.S., Klepikova, A.V., Kulakovskiy, I.V., Gerasimov, E.S., Fedotova, A.V., Besedina, E.G., Kondrashov, A.S., Logacheva, M.D., and Penin, A.A. (2017). High-quality genome assembly of Capsella bursa-pastoris reveals asymmetry of regulatory elements at early stages of polyploid genome evolution. Plant J. **91**:278–291.

Kreiner, J.M., Stinchcombe, J.R., and Wright, S.I. (2018). Population Genomics of Herbicide Resistance: Adaptation via Evolutionary Rescue. Annu. Rev. Plant Biol. **69**:611–635.

Hemanth Kumar, K., Tamatam, A., Pal, A., and Khanum, F. (2013). Neuroprotective effects of Cyperus rotundus on SIN-1 induced nitric oxide generation and protein nitration: ameliorative effect against apoptosis mediated neuronal cell damage. Neurotoxicology **34**:150–159.

Kumar, L., and E Futschik, M. (2007). Mfuzz: a software package for soft clustering of microarray data. Bioinformation **2**:5–7.

Langmead, B. (2010). Aligning short sequencing reads with Bowtie. Curr Protoc Bioinformatics **Chapter 11**. Unit-11.17.

Lati, R.N., Filin, S., and Eizenberg, H. (2011). Temperature-and radiation-based models for predicting spatial growth of purple nutsedge (Cyperus rotundus). Weed sci. **59**:476–482.

Li, B., and Dewey, C.N. (2011). RSEM: accurate transcript quantification from RNA-Seq data with or without a reference genome. BMC Bioinf. **12**:323. 16.

Li, H. (2018). Minimap2: pairwise alignment for nucleotide sequences. Bioinformatics **34**:3094–3100.

Loddo, D., Imperatore, G., Milani, A., Panozzo, S., Farinati, S., Sattin, M., and Zanin, G. (2020). First report of glyphosate-resistant biotype of Eleusine Indica (L.) Gaertn. Europe Agronomy **10**:1692.

Lonhienne, T., Cheng, Y., Garcia, M.D., Hu, S.H., Low, Y.S., Schenk, G., Williams, C.M., and Guddat, L.W. (2022). Structural basis of resistance to herbicides that target acetohydroxyacid synthase. Nat. Commun. **13**:3368.

Lowe, T.M., and Eddy, S.R. (1997). tRNAscan-SE: a program for improved detection of transfer RNA genes in genomic sequence. Nucleic Acids Res. **25**:955–964.

Majoros, W.H., Pertea, M., and Salzberg, S.L. (2004). TigrScan and GlimmerHMM: two open source ab initio eukaryotic gene-finders. Bioinformatics **20**:2878–2879.

McElroy, J.S., and Hall, N.D. (2020). Echinochloa colona with reported resistance to glyphosate conferred by aldo-keto reductase also contains a Pro-106-Thr EPSPS target site mutation. Plant Physiol. **183**:447–450.

Michael, T.P., and VanBuren, R. (2015). Progress, challenges and the future of crop genomes. Curr. Opin. Plant Biol. **24**:71–81.

Mistry, J., Chuguransky, S., Williams, L., Qureshi, M., Salazar, G.A., Sonnhammer, E.L.L., Tosatto, S.C.E., Paladin, L., Raj, S., Richardson, L.J., et al. (2021). Pfam: The protein families database in 2021. Nucleic Acids Res. **49**:D412–D419.

Mohamed, A.I., Beseni, B.K., Msomi, N.Z., Salau, V.F., Erukainure, O.L., Aljoundi, A., and Islam, M.S.; Dynamics (2022). The antioxidant and antidiabetic potentials of polyphenolic-rich extracts of Cyperus rotundus (Linn.). J. Biomol. Struct. Dyn. **40**:12075–12087.

Monson, R.K., and Rawsthorne, S. (2000). CO2 assimilation in C3-C4 intermediate plants. In Photosynthesis: PPhysiology and MMetabolism (Springer), pp. 533–550.

Montgomery, J., Morran, S., MacGregor, D.R., McElroy, J.S., Neve, P., Neto, C., Vila-Aiub, M.M., Sandoval, M.V., Menéndez, A.I., Kreiner, J.M., et al. (2024). Current status of community resources and priorities for weed genomics research. Genome Biol. **25**:139.

Murat, F., Xu, J.-H., Tannier, E., Abrouk, M., Guilhot, N., Pont, C., Messing, J., and Salse, J. (2010). Ancestral grass karyotype reconstruction unravels new mechanisms of genome shuffling as a source of plant evolution. Genome Res. **20**:1545–1557.

Nawrocki, E.P., and Eddy, S.R. (2013). Infernal 1.1: 100-fold faster RNA homology searches. Bioinformatics **29**:2933–2935.

Neeser, C., Aguero, R., and Swanton, C.J. (1997). Survival and dormancy of purple nutsedge (Cyperus rotundus) tubers. Weed sci. **45**:784–790.

Noguera, M.M., Albert, P.S., Saski, C.A., Birchler, J.A., Porri, A., Meiners, I., Lerchl, J., and Roma-Burgos, N. (2024). Extrachromosomal DNA-mediated glutamine synthetase 2 (GS2) amplification enables glufosinate resistance in Amaranthus palmeri. Preprint at bioRxiv. https://doi.org/10.1101/2024.12.13.628355.

Noguera, M.M., Porri, A., Werle, I.S., Heiser, J., Brändle, F., Lerchl, J., Murphy, B., Betz, M., Gatzmann, F., Penkert, M., et al. (2022). Involvement of glutamine synthetase 2 (GS2) amplification and overexpression in Amaranthus palmeri resistance to glufosinate. Planta **256**:57.

O'Donovan, C., Martin, M.J., Gattiker, A., Gasteiger, E., Bairoch, A., and Apweiler, R. (2002). High-quality protein knowledge resource: SWISS-PROT and TrEMBL. Brief. Bioinform. **3**:275–284.

Oerke, E.-C. (2006). Crop losses to pests. J. Agric. Sci. **144**:31–43.

Pan, L., Yu, Q., Han, H., Mao, L., Nyporko, A., Fan, L., Bai, L., and Powles, S. (2019). Aldo-keto reductase metabolizes glyphosate and confers glyphosate resistance in Echinochloa colona. Plant Physiol. **181**:1519–1534.

Pan, L., Yu, Q., Wang, J., Han, H., Mao, L., Nyporko, A., Maguza, A., Fan, L., Bai, L., and Powles, S. (2021). An ABCC-type transporter endowing glyphosate resistance in plants. Proc. Natl. Acad. Sci. USA **118**:e2100136118.

Peerzada, A.M. (2017). Biology, agricultural impact, and management of Cyperus rotundus L.: the world's most tenacious weed. Acta Physiol. Plant. **39**:270.

Peerzada, A.M., Ali, H.H., Naeem, M., Latif, M., Bukhari, A.H., and Tanveer, A. (2015). Cyperus rotundus L.: Traditional uses, phytochemistry, and pharmacological activities. J. Ethnopharmacol. **174**:540–560.

Perotti, V.E., Larran, A.S., Palmieri, V.E., Martinatto, A.K., Alvarez, C.E., Tuesca, D., and Permingeat, H.R. (2019). A novel triple amino acid substitution in the EPSPS found in a high-level glyphosate-resistant Amaranthus hybridus population from Argentina. Pest Manag. Sci. **75**:1242–1251.

Powles, S.B., and Yu, Q. (2010). Evolution in action: plants resistant to herbicides. Annu. Rev. Plant Biol. **61**:317–347.

Price, A.L., Jones, N.C., and Pevzner, P.A. (2005). De novo identification of repeat families in large genomes. Bioinformatics **21**:i351–i358.

Qiao, Y., Zhang, N., Liu, J., and Yang, H. (2023). Interpretation of ametryn biodegradation in rice based on joint analyses of transcriptome, metabolome and chemo-characterization. J. Hazard. Mater. **445**:130526.

Ramirez-Gonzalez, R.H., Borrill, P., Lang, D., Harrington, S.A., Brinton, J., Venturini, L., Davey, M., Jacobs, J., van Ex, F., Pasha, A., et al. (2018). The transcriptional landscape of polyploid wheat. Science **361**:eaar6089.

Rocha, F.G., Brandenburg, M.d.M., Pawloski, P.L., Soley, B.d.S., Costa, S.C.A., Meinerz, C.C., Baretta, I.P., Otuki, M.F., and Cabrini, D.A. (2020). Preclinical study of the topical anti-inflammatory activity of Cyperus rotundus L. extract (Cyperaceae) in models of skin inflammation. J. Ethnopharmacol. **254**:112709.

Sanderson, M.J. (2003). r8s: inferring absolute rates of molecular evolution and divergence times in the absence of a molecular clock. Bioinformatics **19**:301–302.

Seppey, M., Manni, M., and Zdobnov, E.M. (2019). BUSCO: Assessing Genome Assembly and Annotation Completeness. Methods Mol. Biol. **1962**:227–245.

Slater, G.S.C., and Birney, E. (2005). Automated generation of heuristics for biological sequence comparison. BMC Bioinf. **6**:31.

Smit, A., Hubley, R., and Green, P. (1996-2010). RepeatMasker Open-3.0. http://www.repeatmasker.org.

Soltani, N., Dille, J.A., Burke, I.C., Everman, W.J., VanGessel, M.J., Davis, V.M., and Sikkema, P.H. (2016). Potential corn yield losses from weeds in North America. Weed Technol. **30**:979–984.

Srivastava, R.K., Singh, A., and Shukla, S.V. (2013). Chemical investigation and pharmaceutical action of Cyperus rotundus-a review. J. Biol. Act. Prod. Nat. **3**:166–172.

Stamatakis, A. (2014). RAxML version 8: a tool for phylogenetic analysis and post-analysis of large phylogenies. Bioinformatics **30**:1312–1313.

Stanke, M., Keller, O., Gunduz, I., Hayes, A., Waack, S., and Morgenstern, B. (2006). AUGUSTUS: ab initio prediction of alternative transcripts. Nucleic Acids Res. **34**:W435–W439.

Su, Y., Zeeshan Ul Haq, M., Liu, X., Li, Y., Yu, J., Yang, D., Wu, Y., and Liu, Y. (2023). A genome-wide identification and expression analysis of the casparian strip membrane domain protein-like gene family in Pogostemon cablin in response to p-HBA-induced continuous cropping obstacles. Plants **12**:3901.

Sun, Y., Shang, L., Zhu, Q.H., Fan, L., and Guo, L. (2022). Twenty years of plant genome sequencing: achievements and challenges. Trends Plant Sci. **27**:391–401.

Thorvaldsdottir, H., Robinson, J.T., and Mesirov, J.P. (2013). Integrative Genomics Viewer (IGV): high-performance genomics data visualization and exploration. Brief Bioinform **14**:178–192.

Tong, S., Wang, Y., Chen, N., Wang, D., Liu, B., Wang, W., Chen, Y., Liu, J., Ma, T., and Jiang, Y. (2022). PtoNF-YC9-SRMT-PtoRD26 module regulates the high saline tolerance of a triploid poplar. Genome Biol. **23**:148.

Trapnell, C., Williams, B.A., Pertea, G., Mortazavi, A., Kwan, G., van Baren, M.J., Salzberg, S.L., Wold, B.J., and Pachter, L. (2010). Transcript assembly and quantification by RNA-Seq reveals unannotated transcripts and isoform switching during cell differentiation. Nat. Biotechnol. **28**:511–515.

Van de Peer, Y., Mizrachi, E., and Marchal, K. (2017). The evolutionary significance of polyploidy. Nat. Rev. Genet. **18**:411–424.

Wang, H., Fang, T., Li, X., Xie, Y., Wang, W., Hu, T., Kudrna, D., Amombo, E., Yin, Y., Fan, S., et al. (2024). Whole-genome sequencing of allotetraploid bermudagrass reveals the origin of Cynodon and candidate genes for salt tolerance. Plant J. **118**:2068–2084.

Wang, L., Sun, X., Peng, Y., Chen, K., Wu, S., Guo, Y., Zhang, J., Yang, H., Jin, T., Wu, L., et al. (2022). Genomic insights into the origin, adaptive evolution, and herbicide resistance of Leptochloa chinensis, a devastating tetraploid weedy grass in rice fields. Mol. Plant **15**:1045–1058.

Waterhouse, A., Bertoni, M., Bienert, S., Studer, G., Tauriello, G., Gumienny, R., Heer, F.T., de Beer, T.A.P., Rempfer, C., Bordoli, L., et al. (2018). SWISS-MODEL: homology modelling of protein structures and complexes. Nucleic Acids Res. **46**:W296–W303.

Weber, A., and Flügge, U.I. (2002). Interaction of cytosolic and plastidic nitrogen metabolism in plants. J. Exp. Bot. **53**:865–874.

Webster, T.M., and Macdonald, G.E. (2001). A Survey of Weeds in Various Crops in Georgia. Weed Technol. **15**:771–790.

Wu, L.M., Luo, Z., Lu, Y.X., Li, J.Y., Liu, M., Cai, H.L., Zhao, S.Q., Huang, J.H., Yi, L., He, S.F., et al. (2025). Allelic expression dynamics drive herbicide resistance in a devastating triploid weedy grass Cyperus rotundus. Genome Sequence Archive. https://ngdc.cncb.ac.cn/search/all?q=CRA021038.

Xu, Z., and Wang, H. (2007). LTR_FINDER: an efficient tool for the prediction of full-length LTR retrotransposons. Nucleic Acids Res. **35**:W265–W268.

Xue, B.X., He, R.S., Lai, J.X., Mireku-Gyimah, N.A., Zhang, L.H., and Wu, H.H. (2023). Phytochemistry, data mining, pharmacology, toxicology and the analytical methods of Cyperus rotundus L. (Cyperaceae): a comprehensive review. Phytochem. Rev. 1–46.

Yang, J., Ding, C., Xu, B., Chen, C., Narsai, R., Whelan, J., Hu, Z., and Zhang, M. (2015). A Casparian strip domain-like gene, CASPL, negatively alters growth and cold tolerance. Sci. Rep. **5**:14299.

Yang, Z. (1997). PAML: a program package for phylogenetic analysis by maximum likelihood. Comput. Appl. Biosci. **13**:555–556.

Yanniccari, M., Vázquez-García, J.G., Gigón, R., Palma-Bautista, C., Vila-Aiub, M., and De Prado, R. (2022). A novel EPSPS Pro-106-His mutation confers the first case of glyphosate resistance in Digitaria sanguinalis. Pest Manag. Sci. **78**:3135–3143.

Yu, Q., Jalaludin, A., Han, H., Chen, M., Sammons, R.D., and Powles, S.B. (2015). Evolution of a double amino acid substitution in the 5-enolpyruvylshikimate-3-phosphate synthase in Eleusine indica conferring high-level glyphosate resistance. Plant Physiol. **167**:1440–1447.

Zhang, C., Yu, Q., Han, H., Yu, C., Nyporko, A., Tian, X., Beckie, H., and Powles, S. (2022). A naturally evolved mutation (Ser59Gly) in glutamine synthetase confers glufosinate resistance in plants. J. Exp. Bot. **73**:2251–2262.

Zhou, F.Y., Han, H., Han, Y.J., Nyporko, A., Yu, Q., Beckie, H.J., and Powles, S.B. (2023). Aldo-keto reductase may contribute to glyphosate resistance in Lolium rigidum. Pest Manag. Sci. **79**:1528–1537.